Remote Sensing of Environment 323 (2025) 114717

Contents lists available at ScienceDirect

Remote Sensing of Environment

journal homepage: www.elsevier.com/locate/rse

Next generation Arctic vegetation maps: Aboveground plant biomass and woody dominance mapped at 30 m resolution across the tundra biome

Kathleen M. Orndahl [a,*], Logan T. Berner [a], Matthew J. Macander [b], Marie F. Arndal [c], Heather D. Alexander [d], Elyn R. Humphreys [e], Michael M. Loranty [f], Sarah M. Ludwig [g], Johanna Nyman [h], Sari Juutinen [i], Mika Aurela [i], Juha Mikola [j], Michelle C. Mack [k], Melissa Rose [a], Mathew R. Vankoughnett [l], Colleen M. Iversen [m], Jitendra Kumar [n], Verity G. Salmon [o], Dedi Yang [o], Paul Grogan [p], Ryan K. Danby [q], Neal A. Scott [q], Johan Olofsson [r], Matthias B. Siewert [r], Lucas Deschamps [s], Vincent Maire [s], Esther Lévesque [t], Gilles Gauthier [u], Stéphane Boudreau [v], Anna Gaspard [v], M. Syndonia Bret-Harte [w], Martha K. Raynolds [w], Donald A. Walker [w], Anders Michelsen [x], Timo Kumpula [y], Miguel Villoslada [y,1], Henni Ylänne [z], Miska Luoto [aa], Tarmo Virtanen [ab], Heather E. Greaves [ac], Bruce C. Forbes [ad], Ramona J. Heim [ae], Norbert Hölzel [ae], Howard Epstein [af], Andrew G. Bunn [ag], Robert Max Holmes [ah], Susan M. Natali [ah], Anna-Maria Virkkala [ah], Scott J. Goetz [a]

[a] School of Informatics, Computing, and Cyber Systems, Northern Arizona University, Flagstaff, AZ, USA
[b] ABR, Inc.—Environmental Research & Services, Fairbanks, AK, USA
[c] Department of Ecoscience, Aarhus University, Aarhus, Denmark
[d] College of Forestry, Wildlife, and Environment, Auburn University, Auburn, AL, USA
[e] Department of Geography and Environmental Studies, Carleton University, Ottawa, Ontario, Canada
[f] Department of Geography, Colgate University, Hamilton, NY, USA
[g] Department of Earth and Environmental Sciences, Columbia University, Palisades, NY, USA
[h] Jeb E. Brooks School of Public Policy, Cornell University, Ithaca, NY, USA
[i] Finnish Meteorological Institute, Helsinki, Finland
[j] Bioeconomy and Environment Unit, Natural Resources Institute Finland, Helsinki, Finland
[k] Center for Ecosystem Science and Society and Department of Biological Sciences, Northern Arizona University, Flagstaff, AZ, USA
[l] Applied Research, Nova Scotia Community College, Middleton, Nova Scotia, Canada
[m] Climate Change Science Institute, Oak Ridge National Laboratory, Oak Ridge, TN, USA
[n] Environmental Sciences Division, Oak Ridge National Laboratory, Oak Ridge, TN, USA
[o] Environmental Science Division & Climate Change Science Institute, Oak Ridge National Laboratory, Oak Ridge, TN, USA
[p] Department of Biology, Queen's University, Kingston, Ontario, Canada
[q] Department of Geography and Planning, Queen's University, Kingston, Ontario, Canada
[r] Department of Ecology and Environmental Science, Umeå University, Umeå, Sweden
[s] Département des sciences de l'environnement, Université du Québec à Trois-Rivières, Trois-Rivières, Québec, Canada
[t] Département des sciences de l'environnement et Centre d'études nordiques, Université du Québec à Trois-Rivières, Trois-Rivières, Québec, Canada
[u] Centre d'Études Nordiques and Department of Biology, Université Laval, Québec City, Québec, Canada
[v] Département de biologie, Université Laval, Québec City, Québec, Canada
[w] Institute of Arctic Biology, University of Alaska Fairbanks, Fairbanks, AK, USA
[x] Department of Biology, University of Copenhagen, Copenhagen, Denmark
[y] Department of Geographical and Historical Studies, University of Eastern Finland, Joensuu, Finland
[z] School of Forest Sciences, University of Eastern Finland, Joensuu, Finland
[aa] Department of Geosciences and Geography, University of Helsinki, Helsinki, Finland
[ab] Ecosystems and Environment Research Programme, University of Helsinki, Helsinki, Finland
[ac] Department of Natural Resources and Society, University of Idaho, Moscow, ID, USA
[ad] Arctic Centre, University of Lapland, Rovaniemi, Finland
[ae] Institute of Landscape Ecology, University of Münster, Münster, Germany
[af] Department of Environmental Science, University of Virginia, Charlottesville, VA, USA

* Corresponding author at: School of Informatics, Computing, and Cyber Systems, Northern Arizona University, 1295 Knoles Dr, Flagstaff, AZ 86011, USA.
E-mail address: kathleen.orndahl@nau.edu (K.M. Orndahl).

https://doi.org/10.1016/j.rse.2025.114717
Received 5 November 2024; Received in revised form 27 February 2025; Accepted 19 March 2025
Available online 1 April 2025

[ag] Department of Environmental Sciences, Western Washington University, Bellingham, Washington, USA
[ah] Woodwell Climate Research Center, Falmouth, MA, USA

ARTICLE INFO

Edited by Jing M. Chen

Keywords:
Pan Arctic
Plant biomass
Woody plant dominance
Vegetation distribution
Remote sensing
Climate change
Landsat

ABSTRACT

The Arctic is warming faster than anywhere else on Earth, placing tundra ecosystems at the forefront of global climate change. Plant biomass is a fundamental ecosystem attribute that is sensitive to changes in climate, closely tied to ecological function, and crucial for constraining ecosystem carbon dynamics. However, the amount, functional composition, and distribution of plant biomass are only coarsely quantified across the Arctic. Therefore, we developed the first moderate resolution (30 m) maps of live aboveground plant biomass (g m^{-2}) and woody plant dominance (%) for the Arctic tundra biome, including the mountainous Oro Arctic. We modeled biomass for the year 2020 using a new synthesis dataset of field biomass harvest measurements, Landsat satellite seasonal synthetic composites, ancillary geospatial data, and machine learning models. Additionally, we quantified pixel-wise uncertainty in biomass predictions using Monte Carlo simulations and validated the models using a robust, spatially blocked and nested cross-validation procedure. Observed plant and woody plant biomass values ranged from 0 to ~6000 g m^{-2} (mean ≈ 350 g m^{-2}), while predicted values ranged from 0 to ~4000 g m^{-2} (mean ≈ 275 g m^{-2}), resulting in model validation root-mean-squared-error (RMSE) ≈ 400 g m^{-2} and R^2 ≈ 0.6. Our maps not only capture large-scale patterns of plant biomass and woody plant dominance across the Arctic that are linked to climatic variation (e.g., thawing degree days), but also illustrate how fine-scale patterns are shaped by local surface hydrology, topography, and past disturbance. By providing data on plant biomass across Arctic tundra ecosystems at the highest resolution to date, our maps can significantly advance research and inform decision-making on topics ranging from Arctic vegetation monitoring and wildlife conservation to carbon accounting and land surface modeling.

1. Introduction

Aboveground plant biomass and its functional composition (e.g., woody vs. non-woody plants) affect land-atmosphere feedbacks (Chapin et al., 2005; Pearson et al., 2013), wildlife habitat (Skarin et al., 2020; Tape et al., 2018) and land use (Cuerrier et al., 2015), yet our understanding of these climate-sensitive ecosystem attributes remains limited across the rapidly warming Arctic. During the past five decades, the Arctic warmed over three times faster than the rest of the planet (Rantanen et al., 2022), in part due to reductions in spring sea ice and snow cover extent (Serreze and Barry, 2011). Long-term field and satellite measurements indicate warmer and longer growing seasons enabled woody plants (i.e., shrubs and trees) to expand in tundra ecosystems (Dial et al., 2022; Mekonnen et al., 2021), while also widely increasing plant productivity and biomass (Bjorkman et al., 2020; Elmendorf et al., 2012; Epstein et al., 2012; Myers-Smith et al., 2020). These changes signify more carbon storage in plant biomass, with longer carbon residence times in woody plants (DeMarco et al., 2014b; Shaver and Chapin, 1991). However, expansion of taller woody plants over lower-stature plants substantially reduces surface albedo, leading to overall amplification of climate warming (Loranty et al., 2011; Sturm, 2005). Additionally, woody plant expansion is enabling moose (*Alces alces*) and beaver (*Castor canadensis*) to colonize tundra ecosystems (Tape et al., 2018; Tape et al., 2016), while also impacting land use (e.g., hunting, berry picking) in some northern Indigenous communities (Brinkman et al., 2016; Cuerrier et al., 2015). Changes in aboveground plant biomass and woody plant dominance can further alter snow dynamics (Sturm et al., 2001), nutrient cycling (Cahoon et al., 2012; DeMarco et al., 2014a), permafrost stability (Heijmans et al., 2022) and wildfire regimes (Hu et al., 2015). Hence, it is crucial to understand the status of these ecosystem attributes across the Arctic tundra biome.

Aboveground plant biomass has been mapped at moderate to coarse resolution across the entire Arctic; however, additional efforts are needed using more field data and finer spatial resolution satellite data. In seminal work, plant biomass was mapped across the entire Arctic at coarse resolution (8 km) by linking field data from 13 sites with measurements of the Normalized Difference Vegetation Index (NDVI) from the Advanced Very High Resolution Radiometer (AVHRR) satellites (Raynolds et al., 2012). This was the first Arctic-wide map of plant biomass to be derived using satellite data. More recently, Spawn et al. (2020) developed a harmonized global plant biomass dataset that involved mapping plant biomass across the Arctic at moderate resolution (300 m) using Moderate Resolution Imaging Spectroradiometer (MODIS) NDVI and field data from 24 sites in northwestern North American (Berner et al., 2018). These products revealed previously unresolved spatial variability in plant biomass across far northern lands yet had high uncertainty due to limited field data and reliance on coarse resolution satellite measurements of NDVI that are unable to resolve many landscape features (e.g. topographic gradients) and suffer from spectral mixing (e.g., blending terrestrial and aquatic ecosystems in a single pixel). Tundra landscapes are heterogeneous over fine spatial scales with vegetation distribution strongly influenced by topography, hydrology, and permafrost (Frost et al., 2014; Walker et al., 2008), making higher-resolution imagery necessary to accurately capture variation in plant biomass (Lara et al., 2020; Siewert and Olofsson, 2020). Consequently, higher resolution satellites and uncrewed aerial vehicles have been used to map tundra plant biomass at regional (30 m resolution; Berner et al., 2018; Johansen and Tømmervik, 2014; Orndahl et al., 2022b), landscape (2 m - 30 m resolution; Räsänen et al., 2018; Riihimäki et al., 2019; Siewert et al., 2015; Villoslada et al., 2024), and local scales (< 1 cm - 2 cm resolution; Alonzo et al., 2020; Cunliffe et al., 2022; Orndahl et al., 2022a). However, higher-resolution mapping for the entire biome has been constrained by computing and remote sensing capabilities. To better inform ecological analyses, ecosystem modeling, and land management, further efforts are needed to map plant biomass and its functional composition across the entire Arctic at finer spatial resolutions that can resolve landscape heterogeneity.

Several recent advancements have enabled the development of the next generation of plant biomass maps for the Arctic tundra biome. Continued improvement of computing capabilities (e.g. Google Earth Engine; Gorelick et al., 2017) and processing algorithms (e.g., Zhu and Woodcock, 2014) are making it feasible to map global land surface properties at 30 m resolution using Landsat data (e.g., Pekel et al., 2016). Landsat data span the entire Arctic and have revealed the importance of regional climate gradients, surface hydrology, and past disturbances on plant biomass (Berner et al., 2018; Orndahl et al., 2022b). In addition, measurements of plant biomass were recently

[1] Secondary Affiliation: Institute of Agriculture and Environmental Sciences, Estonian University of Life Sciences, Tartu, Estonia

compiled and harmonized by functional type (e.g., shrub) for 636 sites in the Arctic and Sub Arctic (Berner et al., 2024b; Berner et al., 2024a). This is the largest collection of field biomass harvest data compiled to date for the Arctic and will help reduce prior modeling limitations related to sparse field data. A clear opportunity now exists to more accurately quantify plant biomass across the Arctic tundra biome.

Our primary objective was to create maps of live aboveground *plant biomass*, *woody plant biomass* and *woody plant dominance* at 30 m spatial resolution, as well as spatially explicit uncertainty estimates, across the Arctic tundra biome for the year 2020 using field, satellite, and geospatial data linked with machine learning. Henceforth, we use the term *plant biomass* to mean the sum of all live, oven-dried aboveground biomass of bryophytes, forbs, graminoids, shrubs, and trees per square meter of ground surface (g m^{-2}). Similarly, *woody plant biomass* is defined as the sum of all live, aboveground shrub and tree biomass (g m^{-2}). *Woody plant dominance* (%) describes the percentage of aboveground plant biomass that is made up of shrub and tree biomass and is derived by dividing estimates of *woody plant biomass* by estimates of *plant biomass*. Our secondary objectives were to:

1) quantify how these ecosystem attributes varied with bioclimate zone, vegetation community type, and long-term growing season air temperatures (thawing degree days) across the Arctic;
2) generate first-order estimates of belowground plant biomass and carbon stocks for the Arctic;
3) explore the effects of topography, historic wildfire and current permafrost thaw on plant biomass distribution using select case studies.

2. Methods

2.1. Study domain

Our study domain spanned the entire Arctic tundra biome, with a land area of ~8.5 million km^2 (including permanent ice) which comprises ~5.7 % of Earth's total land area (Fig. 1). It includes the High and Low Arctic (henceforth Polar Arctic) and the Oro Arctic, which are treeless alpine areas at high latitudes outside the Polar Arctic (Virtanen et al., 2016). The High Arctic includes bioclimate subzones A, B and C as defined by the Panarctic Flora initiative (PAF, Elvebakk et al., 1999) and has open, very low-stature vegetation and mean July temperatures $\leq$ 7 °C. The Low Arctic includes subzones D and E and has mostly closed vegetation and mean July temperatures $\geq$ 8 and $\leq$ 12 °C (Walker et al., 2005). The mountainous Oro Arctic extends south of the Polar Arctic and has milder, snowier winters (Virtanen et al., 2016). We delineated this domain using tundra ecoregions from the RESOLVE ecoregions dataset (Dinerstein et al., 2017), combined with treeline as defined by the Circumpolar Arctic Vegetation Map (CAVM; CAVM Team, 2003). Although our maps were restricted to Arctic tundra, the coarse delineation of this biome meant some forested areas were included in our study domain. We masked out ocean and inland water using the Joint Research Centre Global Surface Water layer (Pekel et al., 2016), the OpenStreetMap water layer (Yamazaki et al., 2019), and the WorldCover v200 global land cover product (Zanaga et al., 2022); and permanent snow and ice using the Landsat CFMask algorithm and the ice mask product from the Greenland Ice Mapping Project (Howat, 2017; Howat et al., 2014).

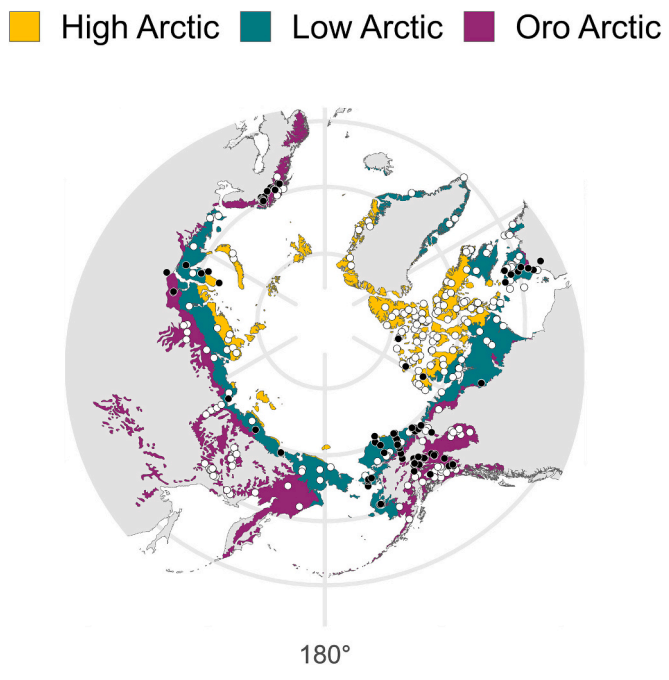

Fig. 1. Pan Arctic study area, divided by bioclimate zone. Field data from the Arctic Plant Aboveground Biomass Synthesis Dataset (Berner et al., 2024a, 2024b) are shown as black dots (n = 256 field sites). User-created vegetation absence data (verified using high-resolution Google Earth satellite imagery) are shown as white dots (n = 218 points). Not all field sites are fully visible due to overplotting.

2.2. Landsat data pre-processing

To produce spectral predictors for modeling biomass, we first created model fits using the Continuous Change Detection and Classification algorithm (CCDC; Zhu and Woodcock, 2014), implemented on Google Earth Engine (GEE, Gorelick et al., 2017). The CCDC algorithm fits harmonic regression models to a time series of reflectance data. The fitted models can then be used to predict reflectance for any date within the time period covered by the input imagery, thus reducing the impact of time series gaps and unreliable shoulder season observations. We fit CCDC models to all usable Landsat 5, 7 and 8 collection 2, tier 1, level 2 data (30 m spatial resolution, henceforth "30 m resolution") from 1984 to 2023. A long time series was necessary to produce reflectance data coincident with field data collection. Before fitting the models, we filtered out Landsat images with extensive cloud cover ($\geq$ 60 %) and low sun angles (peak sun elevation angle $<$ 40° in spring and $<$ 25° in autumn), as well as far northern images with divergent overpass times (worldwide reference system row $>$ 35), resulting in over 200,000 unique images and over 10 trillion multi-band surface reflectance pixel measurements. After filtering images, measurements affected by clouds, cloud shadows, snow, or ice were masked using the CFMask flags, and radiometrically-saturated measurements were masked using the QA_RADSAT band (Foga et al., 2017). Spectral bands and select indices (Table S1) were cross-calibrated across sensors using polynomial regression models that were derived for the Arctic using the *LandsatTS* package for R (Berner et al., 2023). Cross-calibration reduced the absolute mean bias between sensors from 5.7 % $\pm$ 4.9 % to less than 0.6 % $\pm$ 0.6 % (Table S2, S3). All pre-processing steps are listed in Table S4. After pre-processing, the CCDC algorithm was applied to the Landsat data, producing CCDC model fits for each pixel across the study area (Zhu and Woodcock, 2014).

2.3. Modeled seasonal reflectance predictor data

We used the phenological signal from the Landsat data and CCDC model fits to determine pixel-wise days-of-year for each of five seasonal stages: start of the snowfree season, early summer, peak summer, late summer, and end of the snowfree season (Table S5). A time series of all usable Landsat images was sorted by day-of-year, then used to delineate the start of the snowfree season (3rd percentile day-of-year) and the end of the snowfree season (97th percentile day-of-year) for each pixel (Fig. S1). Because snow-covered pixels were masked, these seasons

roughly correspond with the start and end of the snowfree season. To determine days-of-year for peak summer, we used the CCDC model fits to produce modeled NDVI values for each day between June 15th and August 31st, for the years 1985, 1990, 1995, 2000, 2005, 2010, 2015 and 2020. Using the full Landsat time series resulted in better constrained model fits than using only current era data. We then created a pixel-wise maximum NDVI composite for each year, retaining the corresponding day-of-year for each pixel. Finally, we took a median composite of the annual maximum NDVI day-of-year composites and defined this as peak summer (Fig. S2). Early summer was defined as the day-of-year halfway between start of the snowfree season and peak summer, and late summer was defined as the day-of-year halfway between peak summer and end of the snowfree season. These seasonal day-of-year composites allowed us to model reflectance for each seasonal stage using the CCDC model fits (Fig. S3, Fig. S4). We produced Pan Arctic seasonal modeled reflectance images for six Landsat bands (red, green, blue, near infrared (NIR), shortwave infrared 1 (SWIR1) and shortwave infrared 2 (SWIR2)) and five spectral indices (Normalized Difference Moisture Index (NDMI), Normalized Difference Vegetation Index (NDVI), Normalized Difference Wetness Index (NDWI), Enhanced Vegetation Index – 2 band (EVI2b) and Normalized Burn Ratio (NBR); Table S1, S5, S6) for the year 2020 ($n = 55$). For each Landsat band and spectral index, we also calculated a series of annual characteristics including the annual mean, median, and range, and the rate of change between each of the five seasons ($n = 77$, Table S6). To complement the Landsat seasonal reflectance data, our modeling included supplementary predictors such as NDVI texture, permafrost index, ecoregion, latitude, longitude, bioclimate zone, ecosystem type, tree cover and presence, and a series of predictors related to topography ($n = 15$, Table S6).

2.4. Post-hoc topographic correction

Satellite measurements of surface reflectance are influenced by differences in illumination caused by topographic slope and aspect. Topographic correction can compensate for these differences but is typically applied directly to individual Landsat images (Sola et al., 2016) which becomes computationally challenging when using tens of thousands of overlapping images. To reduce computational demands, we developed and applied a 'post-hoc topographic correction' that applies the sun-canopy-sensor+C (SCS + C) method (Soenen et al., 2005) to the modeled reflectance imagery output by the CCDC, rather than to the individual input Landsat images. The SCS + C method corrects for terrain effects on illumination by accounting for the interaction between vegetation canopy and topography, with an additional correction to account for diffuse or low-angle sunlight. This method was developed primarily for forested areas but has been used successfully across a variety of ecosystem types (Moreira and Valeriano, 2014; Yin et al., 2018). Although this method has not, to our knowledge, been tested in Arctic tundra, it performed well across alpine tundra (rocky and grassland areas) in the Spanish Pyrenees (Sola et al., 2016). Further details are provided in the Supplementary Materials (Text S1, Fig. S5).

2.5. Training and validation data

We obtained training and validation data on plant biomass from the Arctic Plant Aboveground Biomass Synthesis Dataset (henceforth 'synthesis dataset'; (Berner et al., 2024a, 2024b)). This harmonized dataset includes measurements of aboveground plant biomass for 636 field sites across the Arctic. Each field site included multiple plots where plant biomass was harvested and partitioned by functional type or, for some tall shrubs and trees, was quantified using stem inventories and allometric models. For each plot, we combined requisite plant functional type biomass to calculate plant (bryophyte, forb, graminoid, shrub, and trees) and woody plant (shrub and tree) biomass density as grams of oven-dried live aboveground biomass per square meter of ground surface (g m^{-2}). The synthesis dataset includes measurements of lichen biomass; however, we excluded lichens from the plant biomass dataset since they are predominately fungal (Allen and Lendemer, 2022), increasingly recognized as a 'complex ecosystem' (Hawksworth and Grube, 2020), and have a different spectral signal from plants (Nelson et al., 2022). For biomass mapping we created two training/validation datasets: one with only plots where all plant biomass was measured, and a second with only plots where all woody plant biomass was measured. The former excluded some plots where, for instance, bryophytes and/or trees were not measured.

The synthesis dataset included very few plots (< 2 %) from unvegetated areas. Therefore, we compiled an additional set of observations with zero biomass (0 g m^{-2}) by generating random points in areas classified as 'Bare/sparse vegetation,' 'Snow and ice' or 'Permanent water bodies' by the 10 m resolution WorldCover v200 global land cover product (Zanaga et al., 2022). To ensure these points were truly unvegetated, we visually examined each using very high-resolution satellite imagery in Google Earth (*Google Earth 9.194.0.0 [WWW Document]*, 2023) and discarded points where vegetation was evident. We additionally checked each 'Bare/sparse vegetation' site for signs of plant phenology by producing NDVI time series using the *LandsatTS* R package (Berner et al., 2023).

Next, we extracted predictor data at each of the plots and unvegetated observations. For Landsat data, seasonal modeled reflectance values were generated based on the exact date of data collection for each plot. Predictor values and biomass were then averaged across plots to aggregate data at the site level (Fig. S6). We assigned site biomass presence/absence using a threshold of 10 g m^{-2} since very sparse amounts of vegetation were unlikely to be detectable in 30 m resolution imagery.

To ensure only the highest quality data were used for model fitting, we performed a series of filtering steps on the calibration/validation data (Table S7). After filtering, our datasets included 223 site-level aboveground plant biomass observations and 256 site-level woody plant aboveground plant biomass observations (Table S8). We retained 218 user-created non-vegetated observations, roughly equivalent to the number of vegetated observations. This allowed for balanced class sizes in our presence/absence classification (see below). The final sample sizes for our modeling effort were $n = 441$ (plant) and $n = 474$ (woody plant).

2.6. Modeling plant biomass

We leveraged random forest models to separately predict aboveground plant biomass (tree, shrub, graminoid, forb and bryophyte biomass) and aboveground woody plant biomass (tree and shrub biomass) using field data for training/validation, and Landsat modeled seasonal reflectance imagery and supplementary spatial data as predictors (Table S6). When modeling vegetation attributes (e.g., biomass, cover), regression models often predict near zero values instead of true zeros (Macander et al., 2022; Orndahl et al., 2022b). Therefore, our modeling framework consisted of two steps: (1) model the presence/absence of plant or woody plant biomass using random forest probability models, and (2) predict plant or woody plant biomass density using random forest regression models. We tested other classification and regression models, including linear regression, support vector machines (SVMs) (Cristianini and Shawe-Taylor, 2000), and gradient boosted models (XGBoost, LightGBM) (Chen and Guestrin, 2016; Ke et al., 2017), but chose random forest (RF) models (Breiman, 2001) based on their overall performance. Models were fitted using the tidymodels framework (Kuhn and Wickham, 2022) in R v4.2.0 (R Core Team, 2020). Further modeling details are found in the Supplementary Materials (Text S2, Tables S9-S14).

Spatial autocorrelation can inflate the perceived accuracy of models (Legendre et al., 2002). To reduce this bias, we spatially blocked the field data when training and evaluating the models. First, we divided the

study area into 100 km x 100 km blocks. This was the spatial autocorrelation sill identified by Macander et al. (2022) for a similar vegetation cover modeling effort that leveraged an order of magnitude more field data (for further details, see Text S3). Then, field data were assigned a spatial block ID corresponding to the block in which they fell (Fig. S6). The spatial blocks (n = 226 plant, n = 237 woody plant) were used as groups during cross-validation such that data from the same block were never split across training and validation sets. Model accuracy was assessed in a nested leave-one-spatial-block-out cross-validation using ten inner folds.

Feature selection and hyperparameter tuning were performed within the nested cross-validation using the minimum redundancy maximum relevance (MRMR) algorithm (Ding and Peng, 2005) and a Latin hypercube parameter grid (McKay et al., 1979), respectively. Classification models were optimized using area under the receiver operating characteristic curve (ROC AUC) (Hand and Till, 2001), and regression models were optimized using the root-mean-square-error (RMSE). The threshold value for the MRMR algorithm was also tuned within the cross-validation, as was the threshold probability for predicting presences in the presence/absence model. The threshold probability was chosen by optimizing the J-Index (Youden, 1950). We assessed model predictor importance using permutation importance, which permutes random values and quantifies the change in model accuracy (Altmann et al., 2010). Final model performance was assessed using overall accuracy, F-Score (Christen and Hand, 2023) and J-Index (Youden, 1950) for classification models and RMSE, mean-absolute error (MAE) and pseudo-R^2 (calculated as the squared correlation between observed and predicted values; hereafter R^2) for regression models. To facilitate model comparison, we also calculated relative RMSE and MAE, which capture RMSE and MAE as a proportion of mean observed biomass.

The tuned models were fitted on the full datasets, imported into GEE using a custom script to convert the R based model fits to GEE readable code (Orndahl and Burns, 2024), and applied across the study area. To combine the classification and regression results, we multiplied results from the presence/absence and regression models. Maps of woody plant dominance were then derived by dividing final mapped estimates of woody plant biomass by plant biomass. Details on the modeling process can be found in Fig. 2.

2.7. Uncertainty analysis

We quantified uncertainty in our map products using Monte Carlo simulations (n = 100) (Berner et al., 2018; Orndahl et al., 2022b). For each simulation, we: (1) randomly sampled with replacement plots/pixels within a site to account for site-level sampling error, (2) randomly sampled with replacement sites within the dataset to account for study area-level sampling error, and (3) permuted modeled seasonal reflectance data using the RMSE from the CCDC model fits to account for error in the Landsat spectral data. We fit models on each permuted dataset following the inner cross-validation procedure in Section 2.6. Feature selection and hyperparameter tuning were performed separately for each Monte Carlo iteration. Each unique model fit was then used to produce a permuted biomass map. For each pixel, we considered the best-estimate of biomass to be the median (50th percentile) across simulations and calculated lower (2.5th percentile) and upper (97.5th percentile) bounds of a 95 % uncertainty interval, as well as relative

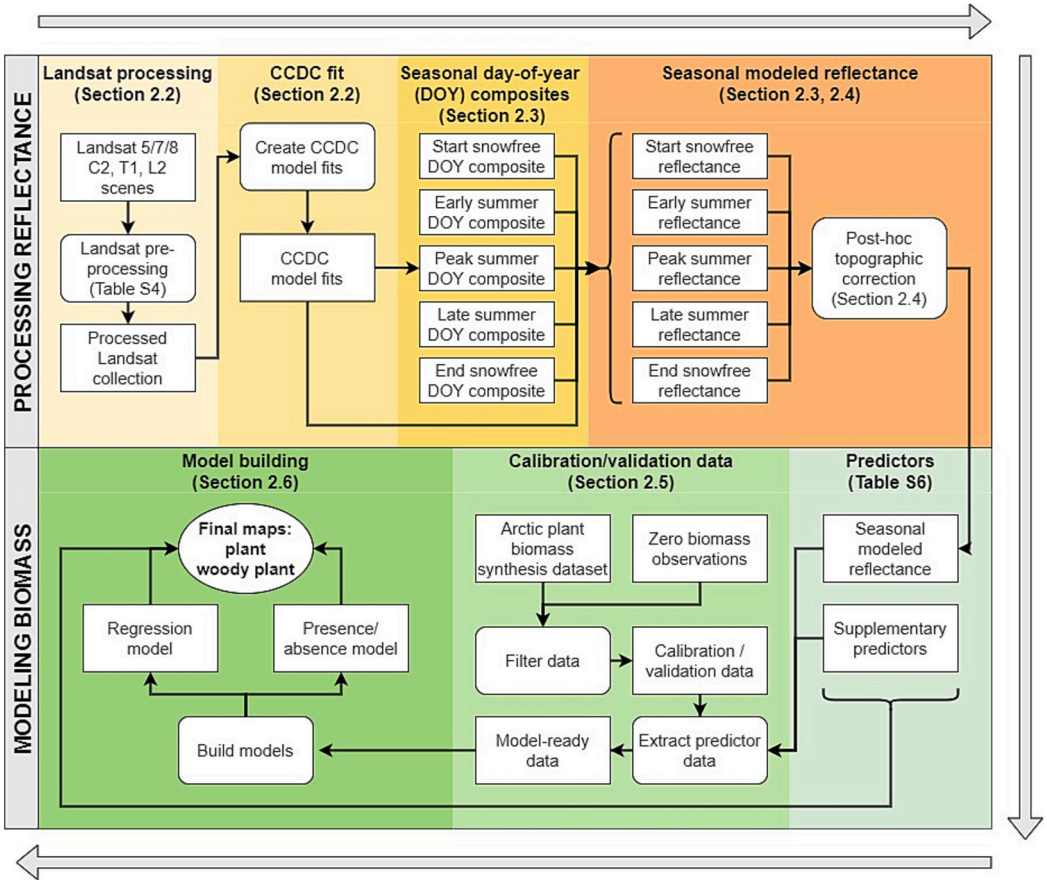

Fig. 2. Flow chart of methodology used to create Pan Arctic biomass maps. The top row (orange) details steps taken to produce seasonal modeled reflectance imagery using Landsat data and the CCDC algorithm. The bottom row (green) details modeling methodology. For each subcategory (shaded boxes), more detailed information can be found in the figures, tables or sections listed. The chart is read clockwise. (For interpretation of the references to colour in this figure legend, the reader is referred to the web version of this article.)

uncertainty ($\frac{95\%\ \text{uncertainty interval}}{\text{median}}$).

2.8. Analysis of plant biomass spatial distribution

We analyzed how the spatial distribution of plant biomass varied geographically and with biological and climatic conditions across the Arctic. To ensure our analysis focused on tundra ecosystems with few trees, we masked out areas with vegetation canopy height ≥ 5 m using a high resolution (1 m) global canopy height map (Meta, World Resources Institute, 2023; Tolan et al., 2024). We chose this threshold for its ability to visually delineate tall shrubs from forest at locations across the study domain and because 5 m is the minimum tree height at maturity for forests used by the United Nations Framework Convention on Climate Change, Convention on Biological Diversity and Global Forest Resources Assessment (FAO, 2002).

After masking out forests, we quantified how total aboveground plant biomass (Tg), average aboveground plant biomass density (g m^{-2}), and woody plant dominance (%) varied across bioclimate zones (Walker et al., 2005) and vegetation community types (Raynolds et al., 2019). When calculating biomass density, we excluded water, ice, permanent snow and other masked areas though included other areas with zero predicted biomass such as rock and bare soil (henceforth "unvegetated"). Furthermore, for these summaries, we calculated woody plant dominance for (1) *all vegetated areas* using the ratio of total (summed) woody plant to plant biomass across each region, and (2) *all land areas* (i.e., vegetated and unvegetated) by averaging pixel-wise woody plant dominance across each region, with non-vegetated areas treated as 0 % woody plant dominance.

To better constrain large-scale estimates of aboveground and belowground plant biomass, and associated carbon stocks, we conducted several analyses. First, we compared our aboveground plant biomass map to existing coarser resolution maps across the Polar Arctic (Raynolds et al., 2012 [8 km]; Spawn and Gibbs, 2020, Spawn et al., 2020) [300 m]). We restricted this comparison to the Polar Arctic (i.e., High + Low Arctic) because Raynolds et al. (2012) did not include the Oro Arctic. Second, we estimated total belowground biomass for the Pan Arctic using our new aboveground biomass map and an assumed belowground: aboveground biomass ratio of 3.7: 1 (Wang et al., 2016). Lastly, we estimated total (belowground + aboveground) plant biomass and its associated carbon stock for the Pan Arctic assuming a biomass carbon content of 0.47 (Paustian et al., 2006).

To illustrate that our new maps capture fine-scale variation in plant biomass across landscapes, including legacies of disturbance, we present several case studies. Specifically, we examined the variation in plant biomass across a historic fire perimeter in Alaska (Jones et al., 2013), active permafrost thaw slumps in Canada (Nitze et al., 2021), and a toposequence in Siberia.

As a first step to evaluating how plant biomass is constrained by climate, we assessed the spatial relationship between plant biomass density and thawing degree days (TDD; 0 °C base). This involved binning the 1 km CHELSA TDD dataset (Karger et al., 2018; Karger et al., 2017) into 10 degree day bins and calculating (1) mean plant and woody plant biomass density and their 95 % uncertainty intervals within each bin and (2) mean woody plant dominance across all land area within the bin. The highest TDD bins represented very little area and were thus susceptible to influence from spurious values and noise in the data. We used the pathviewr (Baliga et al., 2021) package in R to find the elbow in the plotted relationship between TDD bin and area covered, then excluded TDD bins above this elbow. Furthermore, to explore how the relationship between biomass and climate varied among categorical vegetation community types, we calculated the mean plant biomass and mean TDD for each CAVM vegetation community type (Raynolds et al., 2019).

3. Results

3.1. Model accuracy

Field measurements of plant biomass density ranged from 0 to 6260 g m^{-2} (mean: 368 g m^{-2}) and woody plant biomass density ranged from 0 to 6186 g m^{-2} (mean: 252 g m^{-2}). User-created unvegetated points showed little signs of plant phenology and had low mean (± 1 SD) growing season NDVI; 0.11 (0.06) (Fig. S7). We combined presence/absence classification results (accuracy ≥ 95 % for both plant and woody plant biomass, Fig. S8) with regression modeling results to produce final predictions of biomass density. Compared to the field data, the range of predicted values was smaller (0–3886 g m^{-2} for both plant and woody plant biomass), while mean predicted values were similar (plant biomass: 338 g m^{-2}, woody plant biomass: 269 g m^{-2}). Plant and woody plant biomass modeling performed similarly with $R^2 = 0.64$, RMSE = 437 g m^{-2}, MAE = 187 g m^{-2}; and $R^2 = 0.62$, RMSE = 405 g m^{-2}, MAE = 164 g m^{-2}, respectively (Fig. 3a, b). When user created absences were removed from model accuracy assessment, accuracy was reduced to $R^2 = 0.52$, RMSE = 610 g m^{-2}, MAE = 365 g m^{-2} for plant biomass and $R^2 = 0.57$, RMSE = 548 g m^{-2}, MAE = 300 g m^{-2} for woody plant biomass (Table S15). To better assess model performance for low biomass observations, we also calculated accuracy metrics after applying log transformations to the observed data and modeling results. For this assessment, R^2 was heavily influenced by the inclusion of user created absence observations, but RMSE and MAE were relatively stable (Table S15). Plant biomass predictions generally had lower relative RMSE/MAE than woody plant biomass predictions. Topographic correction modestly improved model accuracy (uncorrected results are shown in Fig. S9). For classification models, tree presence, bioclimate zone, and predictors derived from the Normalized Difference Water Index (NDWI) and 2-band Enhanced Vegetation Index (EVI2b) were among the top performers. Regression model top predictors included those derived from NDVI and EVI2b, as well as tree cover and presence, bioclimate zone, ecosystem type and permafrost zonation index (Figs. S10, S11).

3.2. Plant biomass in the Arctic

In 2020, the Arctic tundra biome had 3703 [2159, 6043; 95 % CI] Tg of aboveground plant biomass, with ~72 % of this biomass in woody plants (i.e., shrubs and scattered trees; Table 1, Fig. 4). Across all Arctic land areas, including unvegetated areas, woody plant dominance averaged 41 %. Mean plant and woody plant biomass densities were ~508 g m^{-2} and ~362 g m^{-2}. However, the amount and composition of plant biomass varied markedly among bioclimate zones (Table 1). Most of the plant biomass in the Arctic tundra biome was in the Oro Arctic (~60 %), followed by the Low Arctic (~35 %) and High Arctic (~5 %), with a similar pattern for woody plant biomass (68 % vs. 29 % vs. 3 %). The Oro (38 %) and Low Arctic (39 %) accounted for similar proportions of total Arctic land area, with the High Arctic constituting slightly less (23 %). Therefore, differences in total biomass across bioclimate zones were primarily driven by differences in mean biomass density. For example, mean plant biomass density was ~7 times higher in the Oro Arctic than the High Arctic (~818 g m^{-2} vs. ~115 g m^{-2}), while mean woody plant biomass density was ~15 times higher (~659 g m^{-2} vs. ~45 g m^{-2}, Table 1). Our maps also include 2.7 million km^2 of water, ice and permanent snow that was masked out during the modeling process and assumed to have zero plant and woody plant biomass. Compared to coarser resolution maps, our estimate of total plant biomass for the Polar Arctic was only ~19 % lower than Raynolds et al. (2012); 8 km) and ~ 6 % lower than Spawn and Gibbs, 2020, Spawn et al., 2020); 300 m; Table 2), while pixel-by-pixel comparisons showed decent correspondence ($R^2 \approx 0.5$; Fig. S12).

As a rough approximation for the Arctic tundra biome, we estimate total belowground biomass is ~14 [8.0, 22] Pg. Since total aboveground

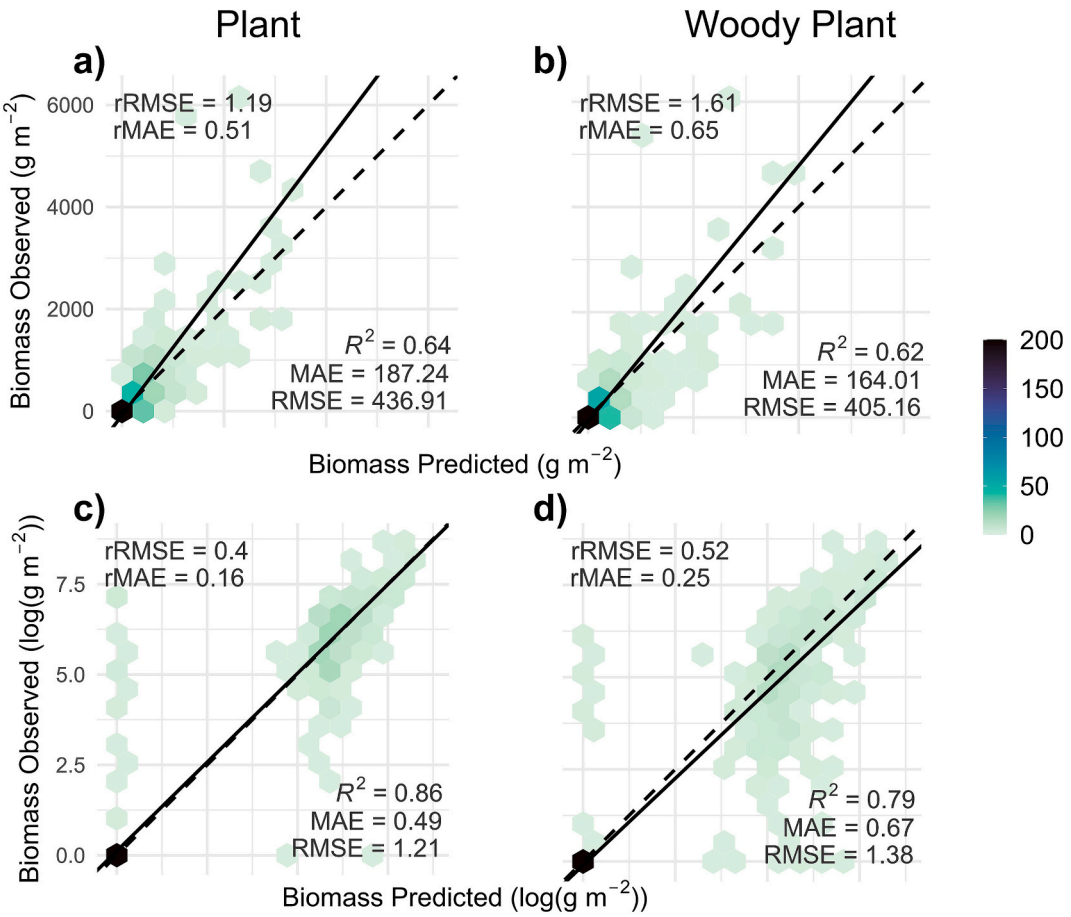

Fig. 3. Comparison of predicted (x-axis) and observed (y-axis) live aboveground biomass for plants (a) and woody plants (b). To better assess predictions for low biomass observations, data were log-log transformed (c, d). All data is plotted, including user created non-vegetated observations. Regression lines (solid black) are fitted using total least squares regression and one-to-one lines are shown as dotted black lines. R^2 is calculated as the squared correlation between observed and predicted values and is thus a 'pseudo- R^2.' To facilitate comparison, relative RMSE (rRMSE) and relative MAE (rMAE) are also reported as $\frac{\text{RMSE/MAE}}{\text{mean(observed biomass)}}$.

Table 1
Aboveground biomass summaries across bioclimate zones. 95 % confidence intervals are shown in brackets. For area and summed biomass totals, the percent of total Pan Arctic area/biomass represented by each bioclimate zone is also listed. Woody dominance is presented as a percentage of both vegetated area and of total land area (% Veg / Land). Water and permanent ice are masked out and not included in area or biomass totals. To exclude forests, areas with canopy height ≥ 5 m are masked out using the Meta Forest Global Canopy Height product (1 m resolution, Meta, World Resources Institute, 2023; Tolan et al., 2024).

			Plant			Woody plant			
Zone	Area (km^2)	%	Summed Biomass (Tg)	%	Biomass Density (gm^{-2})	Summed Biomass (Tg)	%	Biomass Density (gm^{-2})	Woody % Veg / Land
High Arctic	1,875,418	23	168 [88, 295]	5	115 [60, 202]	65 [31, 216]	3	45 [22, 148]	39 / 11
Low Arctic	3,181,389	39	1296 [790, 2081]	35	418 [255, 671]	769 [397, 1735]	29	258 [128, 560]	59 / 38
Oro Arctic	3,053,800	38	2239 [1281, 3667]	60	818 [468, 1339]	1804 [924, 3503]	68	659 [338, 1280]	81 / 59
Pan Arctic	*8,110,607*	*100*	*3703 [2159, 6043]*	*100*	*508 [296, 828]*	*2639 [1353, 5454]*	*100*	*362 [185, 748]*	*71 / 41*

biomass was estimated as 3.7 [2.2, 6.0] Pg, total plant biomass (i.e., aboveground + belowground) may be ~17 [10, 28] Pg. This translates to ~8.2 [4.8, 13] Pg of carbon (C) stored in plant biomass across the biome.

3.3. Differences in plant biomass among vegetation community types

Shrub and graminoid tundra each accounted for about 40 % of all plant biomass in the Polar Arctic, with the remaining plant biomass in wetlands (8 %) and barrens (7 %; Fig. 5, Table S16). Mean plant biomass density was mostly similar among these broad CAVM vegetation community types (400–500 g m^{-2}), except barrens (80 g m^{-2}). However, there were notable differences in mean plant biomass density and woody plant dominance when vegetation community types were split into finer categories (Fig. 5, Table S17). For instance, the southernmost shrub tundras are dominated by shrubs > 40 cm tall and had ~10 times higher mean plant biomass density (~1037 g m^{-2}, CAVM unit S2) than the northernmost shrub tundras which are dominated by prostrate dwarf shrubs (~99 g m^{-2}, CAVM unit P1). Similarly, the southernmost graminoid tundras are composed of tussock sedges, dwarf-shrubs, and

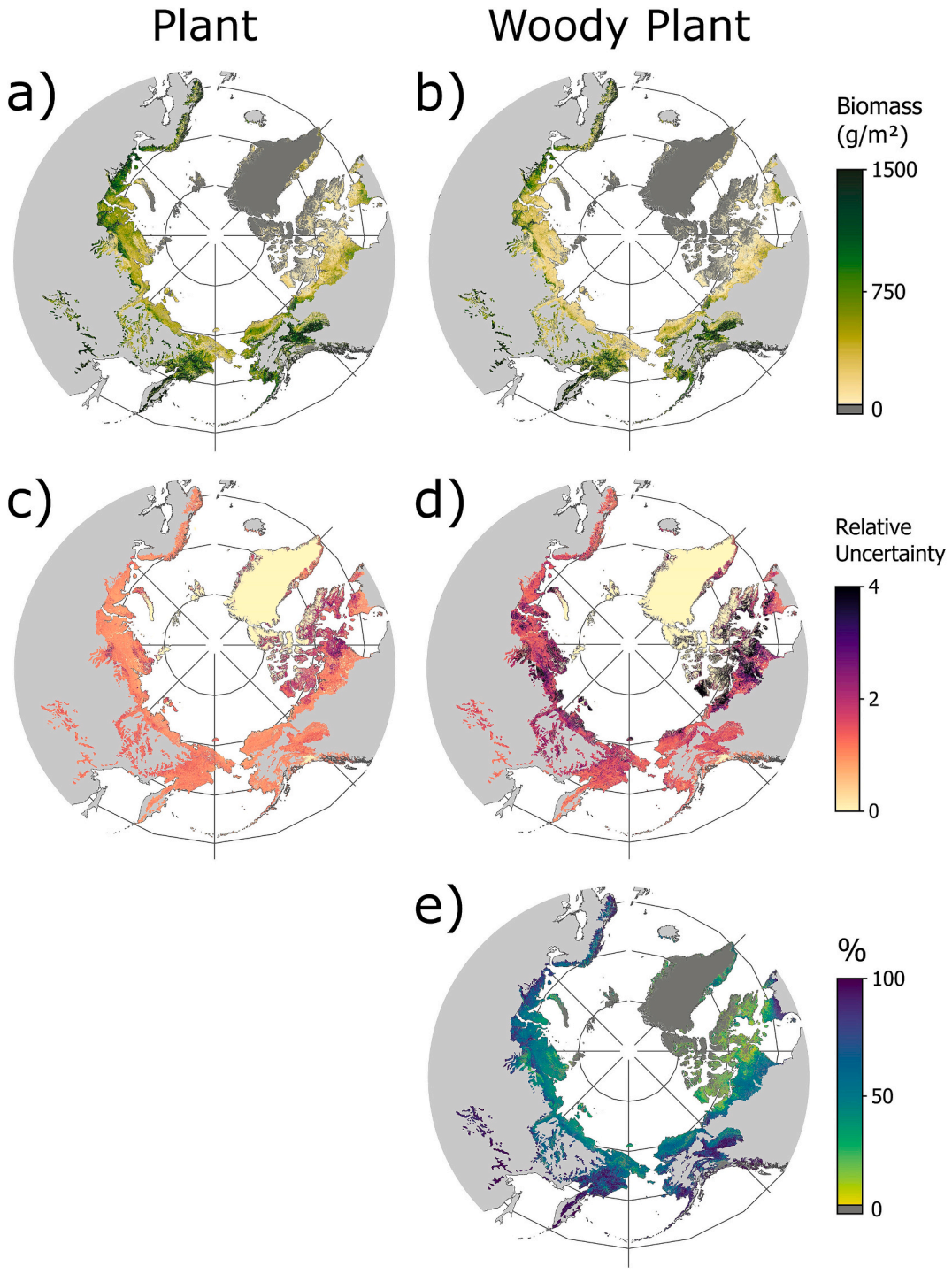

Fig. 4. Aboveground plant biomass (a) and aboveground woody plant (i.e., shrub and tree) biomass (b) mapped across the Pan Arctic. Maps of relative uncertainty ($\frac{95\%\text{ uncertainty interval}}{\text{median}}$) are provided for plant biomass (c) and woody plant biomass (d). Woody dominance ($\frac{\text{woody plant biomass}}{\text{plant biomass}} \times 100$) is shown in (e).

mosses and had about four times higher mean plant biomass density (~507 g m^{-2}, CAVM unit G4) than the northernmost graminoid tundras that are composed of low-growing grasses, rushes, forbs and cryptogams (~119 g m^{-2}, CAVM unit G1). Within both shrub and graminoid tundras, woody plant dominance decreased from the most to the least productive vegetation community types, with low shrub tundra (S2) having the highest mean plant biomass density and woody plant dominance of any non-forest vegetation community type.

3.4. Spatial patterns of plant biomass across the Arctic

Plant biomass hotspots were prevalent in the Oro Arctic, which included some heavily forested and/or Sub Arctic areas due to coarse delineation of the Arctic biome boundaries. Outside the Oro Arctic, higher biomass areas included western Alaska (Seward Peninsula, Yukon-Kuskokwim Delta), the Mackenzie River delta of Canada, and the Nenets region of Russia. These hotspots corresponded with areas of high woody dominance. Uncertainty was highest across the Canadian Shield and the Canadian Arctic Archipelago, and lowest across interior

Table 2
Aboveground biomass summaries comparing the current biomass map product (30 m resolution) to the only other existing Pan Arctic biomass map product from Raynolds et al. (2012); circa 2010, 8 km resolution), and a global biomass map from Spawn and Gibbs, 2020, Spawn et al., 2020; circa 2010, 300 m resolution) across identical areas. 95% confidence intervals are shown in brackets and percentages. For summed biomass totals, the percent of total Pan Arctic biomass represented by each bioclimate zone is also listed. Water and permanent ice are masked out and not included in biomass totals. To exclude forests, areas with canopy height ≥ 5 m are masked out using the Meta Forest Global Canopy Height product (1 m resolution, Meta, World Resources Institute, 2023; Tolan et al., 2024).

	Orndahl (30 m)			Spawn (300 m)			Raynolds (8 km)		
Zone	Sum (Tg)	%	Density (gm^{-2})	Sum (Tg)	%	Density (gm^{-2})	Sum (Tg)	%	Density (gm^{-2})
High Arctic	168 [88, 295]	11	115 [60, 202]	199	13	142	322	18	241
Low Arctic	1296 [790, 2081]	89	418 [255, 671]	1365	87	467	1488	82	506
Pan Arctic	*1464 [877, 2375]*	*100*	*321 [193, 521]*	*1564*	*100*	*362*	*1809*	*100*	*423*

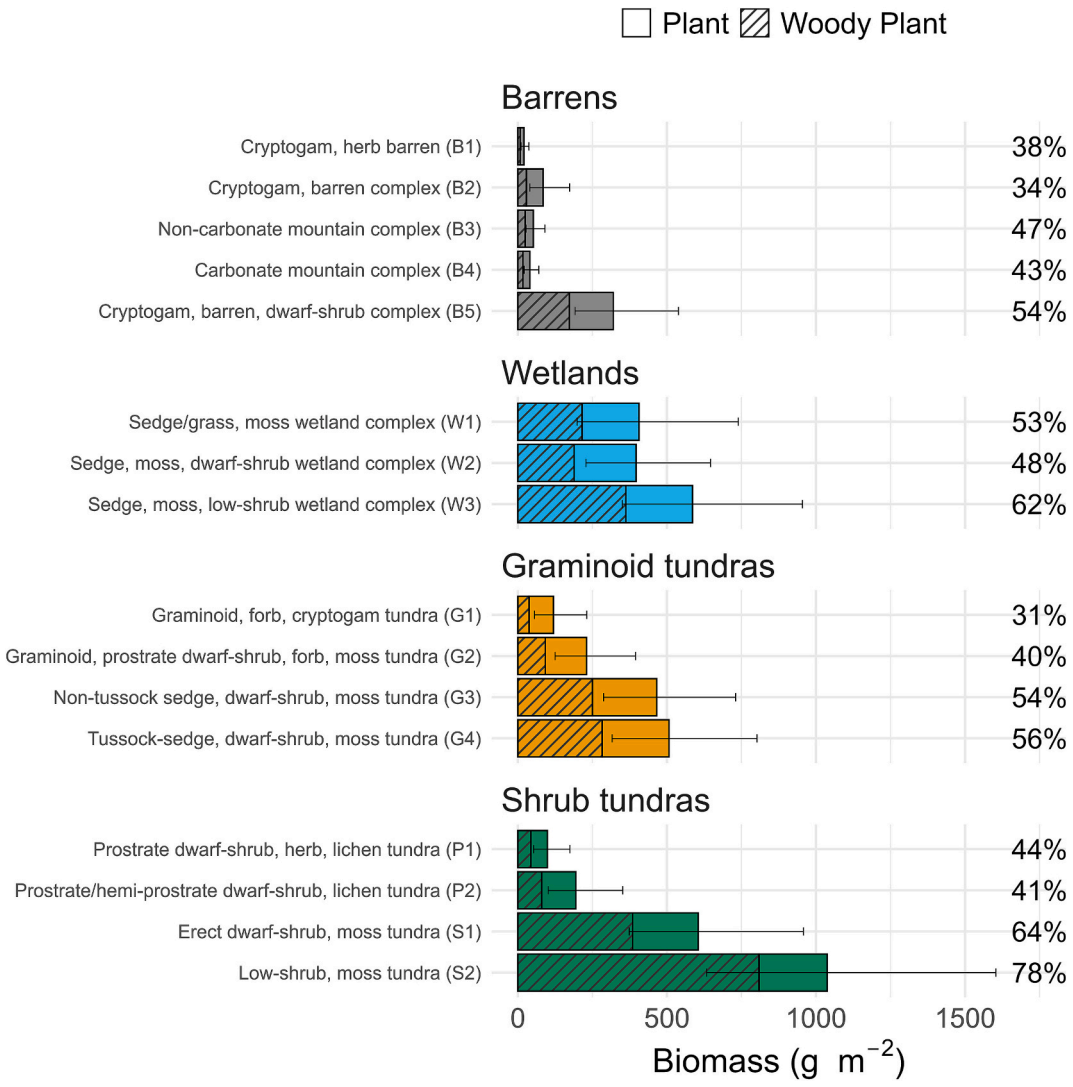

Fig. 5. Average predicted aboveground biomass density within CAVM vegetation community types (Raynolds et al., 2019) across the High and Low Arctic, grouped by broad vegetation category. Woody plant biomass (i.e., shrub and tree) is indicated by hatching, and percent woody plant biomass is displayed to the right of bars. Error bars for plant biomass represent 95% CIs derived from Monte Carlo simulations. Tabular summaries for each vegetation community type are provided in Table S16.

Fennoscandian uplands, Alaska's Seward Peninsula, the Nenets region of Russia, and some areas of interior Yukon Territory and Northwest Territories, Canada (Fig. 4).

While capturing broad differences in plant biomass among bioclimate zones and vegetation community types, our new maps also reveal how plant biomass varies markedly within landscapes, partially due to local topography, surface hydrology and prior disturbances. For instance, pronounced increases in plant biomass and woody plant dominance are evident when transitioning from dry hill tops with minimal vegetation to wet riparian corridors with shrub thickets (Fig. 6). Our new maps also show there is little to no plant biomass in recent permafrost thaw slumps compared to nearby unaffected areas along the Horton River delta, Northwest Territories, Canada (Fig. 7). Conversely, plant biomass and woody plant dominance are

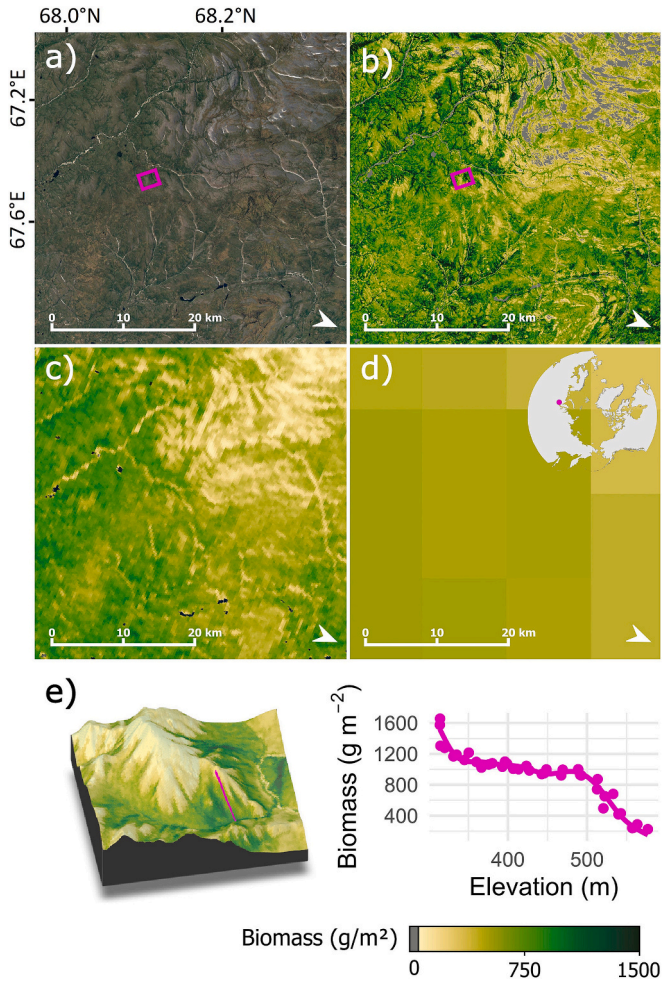

Fig. 6. Spatial patterns of aboveground plant biomass in high-resolution satellite imagery (a), our new 30 m plant biomass map (b), an existing 300 m resolution global plant biomass map (Spawn and Gibbs, 2020, Spawn et al., 2020; c), and an existing 8 km resolution Pan Arctic plant biomass map (Raynolds et al., 2012; d) for an area near the Polar Ural Mountains, Russia. Areas with zero biomass are colored dark grey, and the colour ramp starts at near zero values. Inset (e) shows high-resolution imagery and our 30 m plant biomass map for a focal area with a topographic gradient from lowland riparian corridor to higher elevation ridge top. A transect (pink) laid across this area showed a general decrease in plant biomass as elevation increased, as shown by the plot in the top-right. The high-resolution Google satellite imagery (© 2024 TerraMetrics) was accessed through QGIS (Open Source Geospatial Foundation Project, 2024). (For interpretation of the references to colour in this figure legend, the reader is referred to the web version of this article.)

conspicuously higher inside versus outside the perimeter of a historic fire on the Alaskan North Slope (Fig. 7). These types of spatial variability in plant biomass were not captured in prior plant biomass maps due to their much coarser (300 m - 8 km) spatial resolutions (Fig. 6; Raynolds et al., 2012; Spawn and Gibbs, 2020; Spawn et al., 2020).

3.5. Relationship between plant biomass and growing season temperatures

Mean plant biomass and woody plant biomass increased monotonically with thawing degree days (TDD) across the Arctic (Spearman correlations > 0.9; Fig. 8). Mean plant biomass density increased from < 50 g m^{-2} in the coolest areas (TDD ≤ 150 °C) to ~1200 g m^{-2} in the warmest areas (TDD ≥ 1500 °C), while mean woody plant biomass increased from < 15 g m^{-2} to ~1000 g m^{-2} and woody plant dominance increased from ~2 % to ~85 %. Plant biomass density increased more rapidly once TDD surpassed ~600 °C. A departure from the monotonic increase occurred at ~1600 °C TDD (Fig. 8a), which corresponded primarily with warm but low biomass wetlands in southwestern Alaska. TDD bins ≥ 1810 °C were excluded from analysis, as they represented extreme observations with little spatial coverage that were susceptible to influence from spurious values. The excluded bins constituted < 1 % of total Arctic land area. There was also a positive relationship between average plant biomass density and TDD across CAVM vegetation community types. Shrub tundras had the largest difference in average plant biomass density from the coolest to the warmest regions, whereas wetlands had the smallest range (Fig. 8b).

4. Discussion

4.1. Plant biomass in the Arctic

We mapped plant biomass, woody plant biomass, and woody plant dominance at 30 m resolution across the Arctic tundra biome for the year 2020 using an extensive field dataset, novel satellite remote sensing, and modern machine learning. To create our maps, we used 10–20 times more field data and 100 to > 70,000 times higher spatial resolution satellite data than prior Pan Arctic mapping efforts (Raynolds et al., 2012; Spawn and Gibbs, 2020, Spawn et al., 2020). Furthermore, we provide the first maps of woody plant biomass and woody plant dominance for this biome. Our new maps thus provide unprecedented information on the amount, functional composition, and distribution of plant biomass across the Arctic tundra biome, making them uniquely suited for ecological monitoring and analyses.

The general correspondence between plant biomass quantity/functional composition mapped at 30 m resolution and previously mapped categorical vegetation community types (CAVM Team, 2003; Raynolds et al., 2019) provides confidence that both products are capturing ecologically meaningful patterns despite large discrepancies in spatial and taxonomic resolution. However, the striking similarity in plant biomass density across coarse vegetation community types, despite significant variation within these types, suggests categories such as 'shrub tundra' may be too broad to be ecologically meaningful. For example, 'shrub tundra' includes 'Prostrate dwarf-shrub, herb, lichen tundra' which had some of the lowest biomass densities reported, but also 'Low-shrub, moss tundra' which had the highest biomass densities reported.

Across the Polar Arctic, our estimates of total biomass and biomass density were similar to those tabulated from coarser resolution biomass maps, despite substantial differences in modeling approaches, satellite imagery, and amount of training data. While both prior estimates of total plant biomass fell within our 95 % uncertainty interval, several factors likely explain why our estimate was slightly lower, particularly when compared to Raynolds et al. (2012). First, lichen biomass was included in the two earlier studies, while we excluded it due to its substantial fungal composition and spectral dissimilarity with other plant functional types. The total amount of lichen biomass across the Arctic is unknown, but it comprised an average of 14 % (range: < 1 % to 36 %) of all aboveground biomass at the field sites used by Raynolds et al. (2012) (see Walker et al., 2012). Second, the biomass – NDVI regression model used by Raynolds et al. (2012) did not include training data from unvegetated sites and consequently may have predicted small amounts of biomass across unvegetated area. On the other hand, our two-stage modeling approach and much finer-resolution satellite data helped ensure unvegetated lands were predicted to have zero biomass. Third, the biomass – NDVI regression model used by Raynolds et al. (2012) relied on biomass measurements from field sites with homogenous 'zonal' vegetation and may not extrapolate well where coarse-resolution AVHRR grid cells encompass heterogeneous land cover types. Further comparisons revealed that across the most productive areas of the Polar Arctic, our maps predicted higher plant biomass than Raynolds et al. (2012) but lower plant biomass than Spawn et al. (2020). Raynolds et al. (2012) never predicted plant biomass over 1000 g m^{-2}, possibly due to a

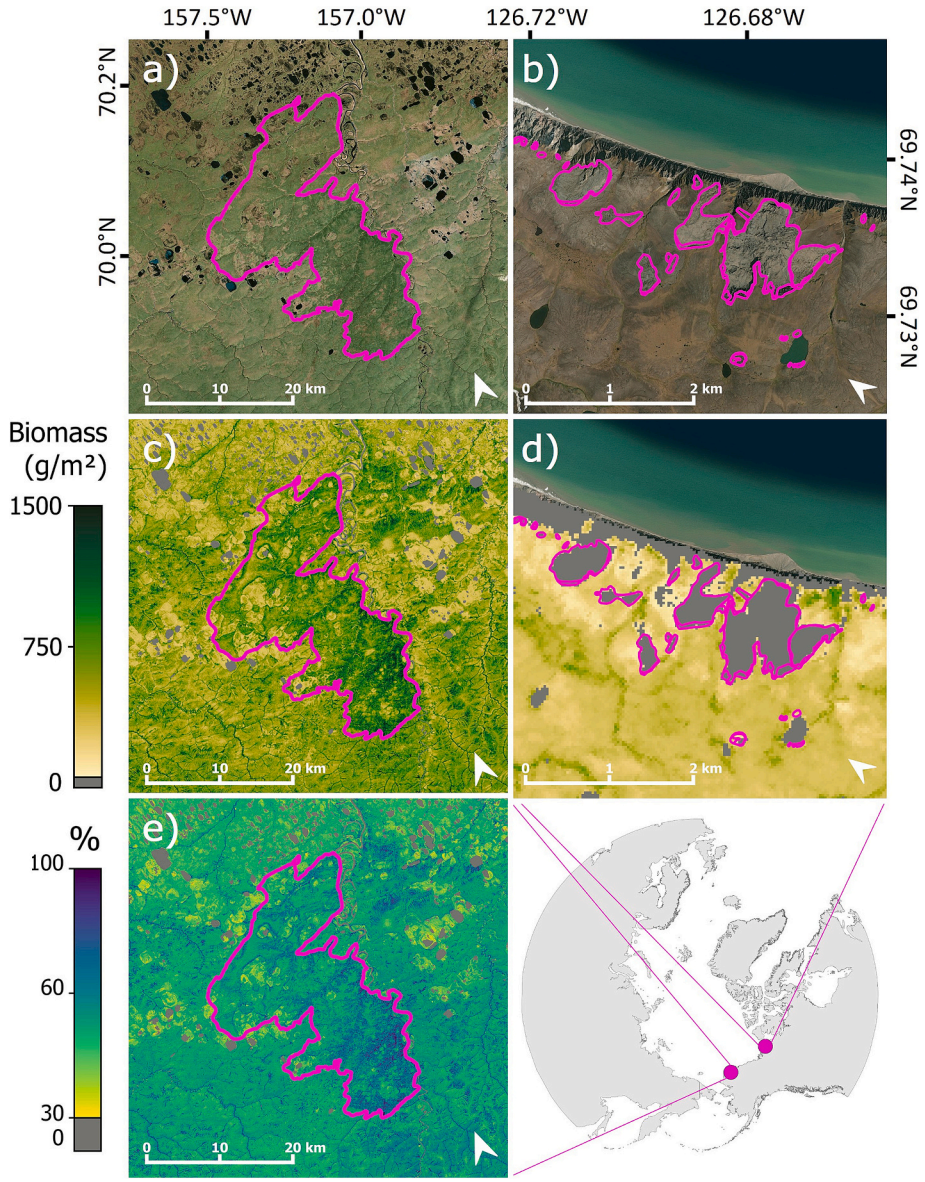

Fig. 7. New 30 m plant biomass maps capture the legacy of disturbances (delimited by pink lines) in the Arctic. The Meade River fire (Jones et al., 2013; a) burned the Alaska North Slope in the late 1800s and shows increased plant biomass (c) and woody plant dominance (e) relative to the surrounding area. Conversely, active thaw slumps along the Horton River delta, Northwest Territories, Canada (Nitze et al., 2021; b) show little to no plant biomass (d). Areas with zero biomass or woody plant dominance are colored grey. The biomass colour ramp starts at near zero values, the woody plant dominance colour ramp starts at 30 %. High resolution imagery was sourced from (a) Bing Maps (© 2024 Microsoft, TomTom, Earthstar Geographics SIO) and (b) ESRI World Imagery (© 2019 Maxar) and was accessed through QGIS (Open Source Geospatial Foundation Project 2024). (For interpretation of the references to colour in this figure legend, the reader is referred to the web version of this article.)

lack of training data in tall shrubs or sparsely treed vegetation communities, whereas Spawn et al. (2020) predicted plant biomass > 5000 g m^{-2} in some instances. Conversely, our maps predicted less biomass across low productivity areas of the Polar Arctic, compared to Raynolds et al. (2012). Overall, it is reassuring that estimates of total plant biomass for the Polar Arctic are broadly consistent among these three datasets.

At the regional level, our maps capture patterns of plant biomass distribution influenced by large-scale processes. For example, high biomass density and woody plant dominance were observed across Fennoscandia which is more temperate than similar latitudes due to the Atlantic meridional overturning circulation, and thus home to more productive vegetation communities (Broecker, 1987). Conversely, biomass density and woody plant dominance were low across the Canadian High Arctic Archipelago, likely due to its relatively recent deglaciation and young landscape age (Raynolds and Walker, 2009). These spatial biomass patterns align with those found in coarser resolution maps from Raynolds et al. (2012) and Spawn et al. (2020).

At the landscape level, our new moderate-resolution maps captured spatial patterns in plant biomass that were not evident in coarser-resolution maps (Raynolds et al., 2012; Spawn and Gibbs, 2020; Spawn et al., 2020). For instance, we found particularly high plant biomass and woody plant dominance in shrub thickets adjacent to rivers, streams, and lakes, as well as hillside gullies and subsurface water channels (i.e., water tracks). Water flow can lead to deeper permafrost thaw depths and higher nutrient availability that support more productive and sometimes shrubbier vegetation in drainages compared with adjacent tundra (Chapin et al., 1988; Curasi et al., 2016; Lamarque et al., 2023; Myers-Smith et al., 2019). These types of landscape features have been hotspots of shrub expansion in recent decades (Naito and

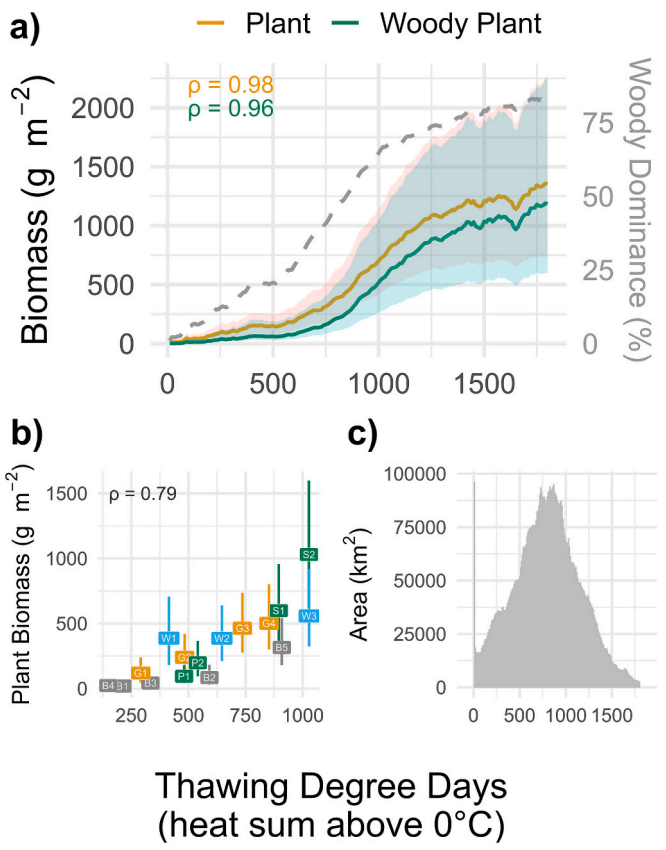

Fig. 8. Average plant biomass density, woody plant biomass density and woody plant dominance increase with thawing degree days along a spatial gradient across the Arctic (a). Thawing degree days (TDD) represent the annual heat sum of all days above 0 °C and are averaged over the period 1981–2010. The TDD data were binned into 10 degree day increments and mean plant and woody plant biomass were calculated for grid cells in each temperature bin (solid lines), as were the 95% confidence intervals across Monte Carlo simulations (shaded ribbons). Pearson correlation coefficients (ρ) between mean TDD and biomass are shown in the upper left. Woody dominance is calculated as a percent of land area by averaging pixel-wise woody dominance values within each bin, with non-vegetated areas treated as 0 % woody dominance. TDD bins > 1800 degree days are excluded as these bins encompassed very little area (< 1 %) and were prone to influence from spurious values. Average plant biomass density increased with TDD across CAVM vegetation community types (b). Colors represent broad vegetation categories where green = shrub tundras, blue = wetlands, orange = graminoid tundras, and grey = barrens. Labels represent vegetation community type codes (Table S16) and error bars show 95% confidence intervals across Monte Carlo simulations. Total area covered per TDD bin roughly followed a normal distribution, although significant area was found in the lowest TDD bin (c). The TDD data are from the 1 km resolution CHELSA Bioclim dataset (Karger et al., 2018, 2017; c). (For interpretation of the references to colour in this figure legend, the reader is referred to the web version of this article.)

Cairns, 2011; Tape et al., 2012). Shrubs can also influence local hydrology by trapping snow, which insulates soils in winter and may increase nutrient cycling (Sturm et al., 2001). The scale at which these interactions play out can be small (10s of meters) with complex spatial patterns that require high- or moderate-resolution imagery to resolve (Siewert and Olofsson, 2020; Villoslada et al., 2024). Therefore, our maps could be used to guide field monitoring of shrub expansion and the combined impacts of vegetation height and topography on local hydrologic regimes and snow dynamics (Bennett et al., 2022).

Our new maps also capture the legacies of disturbances on plant biomass in tundra ecosystems. Thaw slumps can develop when ice-rich permafrost thaws on sloping terrain, leading to vegetation loss and a downslope flow of mud that can continue for decades before stabilizing (Kokelj et al., 2013). Accordingly, our new maps show little to no plant biomass in active thaw slumps in the Horton River delta, Canada (Nitze et al., 2021). Wildfires typically occur over much shorter periods and larger areas than thaw slumps (Foster et al., 2022). However, both disturbances initially decrease plant biomass, followed by a series of successional stages as regrowth occurs. In some cases, disturbance can alter successional trajectories and lead to long-term plant biomass increases, partially due to shrub expansion on exposed mineral soils (Gaglioti et al., 2021; Lantz et al., 2009). Our new maps show conspicuously higher plant biomass and woody plant dominance inside versus outside a ~100-year-old fire boundary on the Alaskan North Slope. This is consistent with field surveys that found vegetation communities were taller and shrubbier in that burned area compared to nearby unburned tundra (Jones et al., 2013). Permafrost degradation, wildfires, and other disturbances (e.g., industrial development) are becoming increasingly common as the Arctic warms (Descals et al., 2022; Forbes et al., 2009; Jorgenson et al., 2006; Lewkowicz and Way, 2019), making it important to understand their short- and long-term impacts on tundra ecosystems. These examples highlight the potential for future analyses of disturbance impacts on plant biomass in tundra ecosystems throughout the Arctic.

We focused our mapping effort on tundra ecosystems. Therefore, our woody plant biomass maps capture predominantly shrub biomass. However, some trees are included along the southern margins of the Low Arctic and at lower elevations in the Oro Arctic due to the relatively coarse delineation of the biome, the complex patchwork of vegetation community types, and the difficulty in applying a precise and consistent definition of forest. While not focused on forests, our training and validation dataset did include some sites with moderate tree biomass, thus our models can capture the biomass of the scattered trees across the Arctic. For instance, some of the world's northernmost trees (*Larix gmelinii* and *cajanderi*) grow within the Russian Low Arctic (Alexander et al., 2012; Kharuk et al., 2023), and these open larch stands are captured by our map as having much higher woody plant biomass (1000–2000 g m^{-2}) than adjacent tundra (< 200 g m^{-2}). However, densely forested areas were outside the scope of our modeling effort. We lacked field data from such areas and therefore likely underestimated their tree biomass and its associated uncertainty. To maintain focus on tundra ecosystems, we masked areas with canopy height ≥ 5 m (Meta, World Resources Institute, 2023; Tolan et al., 2024) when summarizing biomass across the Arctic. Tree masking comes with tradeoffs, however, as no remotely sensed product is perfect. In particular, trees and tall shrubs can be difficult to differentiate, and thus tree masks might inadvertently remove treeless shrublands or other high biomass areas. For this reason, the publicly available map products we provide are unmasked. Users should consider masking forests when working with our plant biomass maps, with careful consideration of which products and thresholds are best for their project goals. To provide consistent estimates of woody plant biomass across high northern latitudes, our map for the Arctic could potentially be harmonized with similar maps for the boreal forest (e.g., Duncanson et al., 2023; Matasci et al., 2018; Wang et al., 2021). Ideally, future mapping would focus on coordinated, collaborative efforts to model the full range of biomass across the Arctic-Boreal domain.

4.2. Novel modeling approaches

Our novel modeling approach leveraged the rich Landsat time series (1984–2023), custom sensor cross-calibration, and a new post-hoc topographic correction. Using the CCDC algorithm to model seasonal reflectance allowed us to fill gaps in the Landsat record (e.g. due to short, cloudy growing seasons and acquisition lapses over Alaska and eastern Siberia during the 1990s; Wulder et al., 2016) and produce robust estimates of shoulder season reflectance. To ensure our Landsat time-series was appropriately standardized, we used cross-sensor calibration models that were specifically developed for the Arctic (Berner

et al., 2023). Finally, we developed a topographic correction method that substantially reduced computational demands while still reducing topographically influenced reflectance artifacts (Fig. S13) and modestly improving the accuracy of biomass models (Fig. S9). Our post-hoc method reduced processing time by approximately 12× compared to applying topographic correction individually to each Landsat image, based on script run-times in Google Earth Engine. Together, these advances in remote sensing enabled us to robustly quantify the amount, functional composition, and distribution of plant biomass at moderate spatial resolution across the Arctic tundra biome.

4.3. Model assessment

Predictors related to modeled seasonal reflectance emerged as highly important according to the permutation importance metric. Seasonal NDWI predictors were most important for biomass presence/absence classification, likely because they differentiate water from other land cover types. Conversely, seasonal NDVI predictors were most important for biomass regression, which is unsurprising given the tight link between NDVI and plant primary productivity (Berner and Goetz, 2022; Tucker and Sellers, 1986). Other predictors with high importance included tree presence and cover and bioclimate zone.

Our models tended to underpredict high biomass observations (e.g. shrub thickets), likely due to limited training data across high biomass areas, and because random forest models cannot extrapolate beyond the response range seen in the training data. At the low biomass end, there were limited instances where moderate biomass was predicted where none was observed. This was likely due to mixed pixels where rock, ice or water was located near higher biomass areas (e.g. lakeside vegetation). Conversely, there were instances where near zero biomass was predicted for areas of relatively high observed biomass (> 1000 g m^{-2}). This was most prevalent for sites from the Canadian Shield with exceptionally high moss biomass, particularly grey-green mats of *Racomitrium* spp. that are likely spectrally similar to rock and bare ground (Gaspard and Boudreau, 2024). This model limitation was further evident in high relative uncertainty across the Canadian Shield and Arctic Archipelago. In general, high latitude and sparsely vegetated areas had high uncertainty, possibly because small patches of mosses and low growing shrubs are difficult to detect in moderate-resolution imagery or are spectrally confused with unvegetated areas.

Unsurprisingly, uncertainty was highest in areas with scarce field and remotely sensed data, such as Western and Eastern Siberia and the Canadian High Arctic, and lowest in areas with abundant data, such as Alaska, Scandinavia and the Nenets region of Russia. Geographic biases in ecological field sampling have caused large portions of Arctic land to be underrepresented, including some of the most rapidly warming regions (Metcalfe et al., 2018; Virkkala et al., 2019). The Arctic Plant Aboveground Biomass Synthesis Dataset (Berner et al., 2024a, 2024b), which formed the basis of our training data, is an important step towards aggregating biomass harvest data across the entire Arctic. However, to further reduce bias in the interpretations drawn from Arctic research, more work is needed to standardize field sampling methods and increase sampling efforts in underrepresented areas.

We aimed to model uncertainty according to best practices (Duncanson et al., 2021), but acknowledge that not all sources of uncertainty are captured here. For example, we were unable to find estimates of error inherent in the biomass harvest and drying processes, although we suspect this error is significant. The intermixing of dwarf shrubs, lichens and mosses makes it difficult to successfully separate and harvest all biomass at a plot. Furthermore, errors can arise from the accidental inclusion of dead biomass, belowground biomass, and/or biomass from outside the plot. There is also error inherent in remotely sensed data. We captured some of this error using the RMSE from the CCDC model fits but recognize there is error in the Landsat imagery and other remotely sensed predictors for which we do not account. In addition, scaling from very small harvest plots (typically < 1 m^2) to moderate-resolution satellite imagery (30 m) can introduce biases that influence model results (Siewert and Olofsson, 2020). As advances in computation continue to facilitate mapping efforts, thorough and transparent uncertainty assessment will be crucial to product comparability (Duncanson et al., 2021).

4.4. Belowground biomass and carbon stocks

We focused on aboveground biomass; yet belowground biomass tends to account for most of the plant biomass in tundra ecosystems (Iversen et al., 2015; Shaver and Chapin, 1991). However, mapping belowground biomass is challenging because optical satellites cannot directly measure belowground characteristics, and there are limited field data. We estimate Arctic belowground biomass totals roughly 14 [8.0, 22] Pg. This translates to roughly 17 [10, 28] Pg of total plant biomass (aboveground + belowground), and roughly 8.2 [4.8, 13] Pg of plant carbon (C). Surface soil organic matter (0–30 cm depth) stores ~53 Pg C in this biome (Poggio et al., 2021), suggesting total ecosystem carbon stocks are ~61 Pg C, with ~13 % in plant biomass, though these estimates do not include forested areas or the large soil carbon stocks deeper than 30 cm (Schuur et al., 2022). For the Polar Arctic, our estimates are surprisingly consistent with Spawn et al. (2020) for total belowground biomass (~5.4 [3.2, 8.8] Pg vs ~5.7 Pg) and total plant biomass (~6.9 [4.1, 11] Pg vs. ~7.3 Pg). Despite this agreement, there is substantial uncertainty in estimates of total plant biomass and its belowground component across the Arctic as evidenced by the wide uncertainty intervals and large range of estimates historically provided for belowground to aboveground biomass ratios (Jackson et al., 1996; Mokany et al., 2006; Wang et al., 2016). It may be possible to derive more rigorous estimates by using our maps to partition aboveground biomass for woody versus non-woody plants and then applying belowground to aboveground biomass ratios for these broad plant functional types (Iversen et al., 2015). Alternatively, our aboveground biomass maps could be combined with information on the spatial distribution of vegetation community types (e.g., Raynolds et al., 2019) and their respective belowground to aboveground biomass ratios. Improved understanding of belowground biomass is important not only for fuller accounting of carbon stocks, but also because the belowground growing season is often much longer than the aboveground growing season (Blume-Werry et al., 2016), with implications for nutrient acquisition and plant responses to a changing climate (Riley et al., 2021).

4.5. Relationship between biomass and climate

Plant and woody plant biomass increased with thawing degree days (TDD), consistent with decades of research tying Arctic warming with enhanced vegetation greenness and productivity (Berner et al., 2020; Elmendorf et al., 2012; Myers-Smith et al., 2015; Myneni et al., 1997). However, inflection points were evident around 600 °C TDD, possibly as functional composition shifts towards woody plants, and again around 1250 °C TDD, suggesting possible saturation points in either vegetation responses to warming temperatures (Elmendorf and Hollister, 2023; Piao et al., 2014) or model predictions in productive areas. The range of biomass across the TDD gradient was considerable, from cold areas with limited vascular plant growth, to coastal areas where warm ocean currents support a temperate climate and high plant productivity (Broecker, 1987). In the warmest areas of the Arctic, mean plant biomass was dominated almost entirely by shrubs and scattered trees. As the Arctic warms, the distribution of Arctic land area will likely shift towards higher TDD bins, with probable increases in woody plant dominance (Mekonnen et al., 2018; Pearson et al., 2013). Across vegetation community types, shrub tundra plant biomass was an order of magnitude higher in the warmest Arctic regions (> 1000 g m^{-2} in low-shrub tundra) versus the coolest regions (~100 g m^{-2} in prostrate dwarf-shrub tundra, Fig. 8c). This suggests a tight link between growing season temperature and shrub growth (Elmendorf et al., 2012) and highlights

the shortcomings of coarse vegetation classes e.g. 'shrub tundra' which are frequently utilized to map and summarize Arctic vegetation (Coops and Wulder, 2019; Cushman et al., 2010). In contrast, wetlands had similar amounts of plant biomass regardless of TDD, suggesting wetland productivity may be governed by factors besides growing season temperature (but see Gauthier et al., 2013) or our models may not be well constrained for predicting wetland biomass.

4.6. Potential applications

Biogeochemistry and ecosystem models are important tools for understanding climate change impacts in the Arctic (Mekonnen et al., 2021; Yu et al., 2017). As such, there is a pressing need to evaluate models against observational datasets related to plant biomass (Fisher et al., 2018; Sulman et al., 2021). Our new biomass maps are well-suited for model evaluation, since we quantified uncertainty for each grid cell. Additionally, our maps provide detailed information that could be invaluable as model inputs. Well constrained spatial biomass estimates could improve future carbon flux models (Virkkala et al., 2021), while detailed data on woody plant distribution could facilitate wildlife habitat modeling. For example, moose (*Alces alces*), beaver (*Castor canadensis*), and canopy arthropods rely on tall shrubs (Sweet et al., 2015; Tape et al., 2018; Zhou et al., 2020), while caribou (*Rangifer tarandus*) might avoid them because they impede movement, hide predators, and outcompete preferred forage such as lichens (Fauchald et al., 2017; Rickbeil et al., 2018). Altogether, the moderate spatial resolution and carefully constrained uncertainty of our maps make them useful for myriad ecological applications.

5. Conclusion

We benchmarked aboveground plant biomass and woody plant dominance across the Arctic for the year 2020 at 30 m spatial resolution using field, satellite, and ancillary spatial data linked with machine learning in a cloud-computing environment. These new maps reveal local (e.g., topography, disturbance) and regional (e.g., climate) factors shaping the amount, composition, and distribution of plant biomass across the Arctic, making them well suited for further ecological analyses and an important step forward. Nevertheless, future efforts will be needed to further improve characterization of plant biomass across the Arctic, including by using more extensive and better standardized field data, and advanced airborne and satellite remote sensing. The modeling framework we developed could additionally be leveraged to assess changes across the four-decade Landsat record and provide real-time insights into tundra ecosystem attributes. Sustained efforts will be necessary to map and assess ongoing transformation of tundra ecosystems as continued warming drives further permafrost thaw, wildfires, and shrub and tree expansion.

CRediT authorship contribution statement

Kathleen M. Orndahl: Writing – review & editing, Writing – original draft, Visualization, Validation, Supervision, Software, Resources, Project administration, Methodology, Investigation, Formal analysis, Data curation, Conceptualization. **Logan T. Berner:** Writing – review & editing, Writing – original draft, Visualization, Validation, Supervision, Project administration, Methodology, Investigation, Funding acquisition, Formal analysis, Data curation, Conceptualization. **Matthew J. Macander:** Writing – review & editing, Software, Methodology. **Marie F. Arndal:** Writing – review & editing, Data curation. **Heather D. Alexander:** Writing – review & editing, Data curation. **Elyn R. Humphreys:** Writing – review & editing, Data curation. **Michael M. Loranty:** Writing – review & editing, Data curation. **Sarah M. Ludwig:** Writing – review & editing. **Johanna Nyman:** Writing – review & editing, Data curation. **Sari Juutinen:** Writing – review & editing, Data curation. **Mika Aurela:** Writing – review & editing, Data curation. **Juha Mikola:** Writing – review & editing, Data curation. **Michelle C. Mack:** Writing – review & editing, Data curation. **Melissa Rose:** Writing – review & editing, Data curation. **Mathew R. Vankoughnett:** Writing – review & editing, Data curation. **Colleen M. Iversen:** Writing – review & editing, Data curation. **Jitendra Kumar:** Writing – review & editing, Data curation. **Verity G. Salmon:** Writing – review & editing, Data curation. **Dedi Yang:** Writing – review & editing, Data curation. **Paul Grogan:** Writing – review & editing, Data curation. **Ryan K. Danby:** Writing – review & editing, Data curation. **Neal A. Scott:** Writing – review & editing, Data curation. **Johan Olofsson:** Writing – review & editing, Data curation. **Matthias B. Siewert:** Writing – review & editing, Data curation. **Lucas Deschamps:** Writing – review & editing, Data curation. **Vincent Maire:** Writing – review & editing, Data curation. **Esther Lévesque:** Writing – review & editing, Data curation. **Gilles Gauthier:** Writing – review & editing, Data curation. **Stéphane Boudreau:** Writing – review & editing, Data curation. **Anna Gaspard:** Writing – review & editing, Data curation. **M. Syndonia Bret-Harte:** Writing – review & editing, Data curation. **Martha K. Raynolds:** Writing – review & editing, Data curation. **Donald A. Walker:** Writing – review & editing, Data curation. **Anders Michelsen:** Writing – review & editing, Data curation. **Timo Kumpula:** Writing – review & editing, Data curation. **Miguel Villoslada:** Writing – review & editing, Data curation. **Henni Ylänne:** Writing – review & editing, Data curation. **Miska Luoto:** Writing – review & editing, Data curation. **Tarmo Virtanen:** Writing – review & editing, Data curation. **Heather E. Greaves:** Writing – review & editing, Data curation. **Bruce C. Forbes:** Writing – review & editing, Data curation. **Ramona J. Heim:** Writing – review & editing, Data curation. **Norbert Hölzel:** Writing – review & editing, Data curation. **Howard Epstein:** Writing – review & editing, Data curation. **Andrew G. Bunn:** Writing – review & editing, Data curation. **Robert Max Holmes:** Writing – review & editing, Data curation. **Susan M. Natali:** Writing – review & editing, Data curation. **Anna-Maria Virkkala:** Writing – review & editing, Data curation. **Scott J. Goetz:** Writing – review & editing, Supervision, Project administration, Funding acquisition, Conceptualization.

Declaration of competing interest

The authors declare that they have no known competing financial interests or personal relationships that could have appeared to influence the work reported in this paper.

Acknowledgements

We thank Dr. Andrew Cunliffe and two anonymous reviewers for constructive and thoughtful feedback during peer review. This material is based upon work supported by the National Aeronautics and Space Administration (NASA) Early Career Investigator Program in Earth Science (Grant No. 80NSSC21K1364 to LTB), the National Science Foundation (NSF) Navigating the New Arctic Program (Grant No. 2127273 to LTB and SJG), and the NASA Arctic Boreal Vulnerability Experiment (ABoVE; Grant No. 80NSSC22K1247 to SJG and LTB). We thank Google for providing additional computing resources on Earth Engine.

Further support was provided by US, Canadian, and European entities. HEG acknowledges support from the NASA Terrestrial Ecology Program (Grant No. NNX12AK83G) and NASA Earth Science Fellowship (Grant No. NNX15AP04H). HE acknowledges support from the NASA Land Cover Land Use Change Program and NSF Biocomplexity Program. MML acknowledges support from the NSF Office of Polar Programs (OPP; Grant No. 1417745). MCM acknowledges support from the NSF Division of Environmental Biology (DEB; Grant No. DEB-2224776 and DEB-1636476). MSB-H acknowledges support from NSF OPP (Grant No. 1936752) and NSF DEB (Grant No. 1556481). CMI, VGS, and JK acknowledge support from The Next Generation Ecosystem Experiments in the Arctic (NGEE Arctic) project that is supported by the Biological

and Environmental Research Program in the Department of Energy's Office of Science.

Canadian entities provided support for this research. ERH acknowledges support from POLAR Knowledge Canada (POLAR) and Natural Sciences and Engineering Research Council of Canada (NSERC). NAS acknowledges support from the Northern Scientific Training Program (NSTP), International Polar Year (IPY), NSERC, ArcticNet, and Queen's University. EL acknowledges support from the Fonds de Recherche du Québec-Nature et technologies (Grant No. FRQNT-2018- PR- 208107), NSERC Discovery Program, and Natural Resources Canada Polar Continental Shelf Program (NRC PCSP). GG acknowledges support from the FRQNT, NSERC, POLAR, ArcticNet, NRC PCSP, and Faculté des sciences de l'agriculture et de l'alimentation of Université Laval. SB acknowledges support from the Québec Ministère de la Forêt, de la Faune et des Parcs.

European entities provided further support for this research. AM acknowledges support from the Independent Research Fund Denmark (Grant No. 0135-00140B and 2032-00064B). MBS acknowledges support from the European Union (ILLUQ) and Swedish Research Council (Grant No. 2021-05767). A-MV acknowledges support from the Otto Malm foundation, Nordenskiöld samfundet, and Societas Pro Fauna et Flora Fennica. JM acknowledges support from the Academy of Finland, Finnish Center of Excellence Program, and EU FP7. The Academy of Finland also supported TK and MV (Grant No. 330319), HY (Grant No. 330845), and ML (Grant No. 1342890). BCF acknowledges support from the European Commission Research and Innovation (CHARTER; Grant No. 869471).

Appendix A. Supplementary material

Supplementary material to this article can be found online at https://doi.org/10.1016/j.rse.2025.114717.

Data availability

Data and novel statistical code pertinent to the results presented in this publication are archived in a public GitHub repository: https://doi.org/10.5281/zenodo.15059170 (Orndahl, 2025). Gridded map data are archived in a public Arctic Data Center dataset: https://doi.org/10.18739/A2NS0M06B (Orndahl et al., 2024).

References

Alexander, H.D., Mack, M.C., Goetz, S., Loranty, M.M., Beck, P.S.A., Earl, K., Zimov, S., Davydov, S., Thompson, C.C., 2012. Carbon accumulation patterns during Post-fire succession in Cajander larch (Larix cajanderi) forests of Siberia. Ecosystems 15, 1065–1082. https://doi.org/10.1007/S10021-012-9567-6/TABLES/4.

Allen, J.L., Lendemer, J.C., 2022. A call to reconceptualize lichen symbioses. Trends Ecol. Evol. 37, 582–589. https://doi.org/10.1016/j.tree.2022.03.004.

Alonzo, M., Dial, R.J., Schulz, B.K., Andersen, H.E., Lewis-Clark, E., Cook, B.D., Morton, D.C., 2020. Mapping tall shrub biomass in Alaska at landscape scale using structure-from-motion photogrammetry and lidar. Remote Sens. Environ. 245, 111841. https://doi.org/10.1016/j.rse.2020.111841.

Altmann, A., Toloşi, L., Sander, O., Lengauer, T., 2010. Permutation importance: a corrected feature importance measure. Bioinformatics 26, 1340–1347. https://doi.org/10.1093/BIOINFORMATICS/BTQ134.

Baliga, V.B., Armstrong, M.S., Press, E.R., 2021. pathviewR: tools to import, clean, and visualize animal movement data in R. Github Repos. https://doi.org/10.5281/zenodo.4270187.

Bennett, K.E., Miller, G., Busey, R., Chen, M., Lathrop, E.R., Dann, J.B., Nutt, M., Crumley, R., Dillard, S.L., Dafflon, B., Kumar, J., Bolton, W.R., Wilson, C.J., Iversen, C.M., Wullschleger, S.D., 2022. Spatial patterns of snow distribution in the sub-Arctic. Cryosphere 16, 3269–3293. https://doi.org/10.5194/TC-16-3269-2022.

Berner, L.T., Goetz, S.J., 2022. Satellite observations document trends consistent with a boreal forest biome shift. Glob. Chang. Biol. 28, 3275–3292. https://doi.org/10.1111/GCB.16121.

Berner, L.T., Jantz, P., Tape, K.D., Goetz, S.J., 2018. Tundra plant above-ground biomass and shrub dominance mapped across the north slope of Alaska. Environ. Res. Lett. 13. https://doi.org/10.1088/1748-9326/aaaa9a.

Berner, L.T., Massey, R., Jantz, P., Forbes, B.C., Macias-Fauria, M., Myers-Smith, I.H., Kumpula, T., Gauthier, G., Andreu-Hayles, L., Gaglioti, B.V., Burns, P., Zetterberg, P., D'Arrigo, R., Goetz, S.J., 2020. Summer warming explains widespread but not uniform greening in the Arctic tundra biome. Nat. Commun. 111 (11), 1–12. https://doi.org/10.1038/s41467-020-18479-5.

Berner, L.T., Assmann, J.J., Normand, S., Goetz, S.J., 2023. "LandsatTS": an R package to facilitate retrieval, cleaning, cross-calibration, and phenological modeling of Landsat time series data. Ecography (Cop.) 2023, e06768. https://doi.org/10.1111/ECOG.06768.

Berner, L.T., Orndahl, K.M., Rose, M., Tamstorf, M., Arndal, M.F., Alexander, H.D., Humphreys, E.R., Loranty, M.M., Ludwig, S.M., Nyman, J., Juutinen, S., Aurela, M., Happonen, K., Mikola, J., Mack, M.C., Vankoughnett, M.R., Iversen, C.M., Salmon, V. G., Yang, D., Kumar, J., Grogan, P., Danby, R.K., Scott, N.A., Olofsson, J., Siewert, M. B., Deschamps, L., Lévesque, E., Maire, V., Morneault, A., Gauthier, G., Gignac, C., Boudreau, S., Gaspard, A., Kholodov, A., Bret-Harte, M.S., Greaves, H.E., Walker, D., Gregory, F.M., Michelsen, A., Kumpula, T., Villoslada, M., Ylänne, H., Luoto, M., Virtanen, T., Forbes, B.C., Hölzel, N., Epstein, H., Heim, R.J., Bunn, A., Holmes, R. M., Hung, J.K.Y., Natali, S.M., Virkkala, A.M., Goetz, S.J., 2024a. The Arctic plant aboveground biomass synthesis dataset. Sci. Data 111 (11), 1–13. https://doi.org/10.1038/s41597-024-03139-w.

Berner, L.T., Orndahl, K.M., Rose, M., Tamstorf, M., Arndal, M.F., Alexander, H.D., Yang, D., Humphreys, E.R., Loranty, M.M., Ludwig, S.M., Nyman, J., Juutinen, S., Aurela, M., Happonen, K., Mikola, J., Mack, M.C., Vankoughnett, M.R., Iversen, C. M., Salmon, V.G., Kumar, J., Grogan, P., Danby, R.K., Scott, N.A., Olofsson, J., Siewert, M.B., Deschamps, L., Lévesque, E., Maire, V., Morneault, A., Gauthier, G., Gignac, C., Boudreau, S., Gaspard, A., Kholodov, A., Bret-Harte, M.S., Greaves, H.E., Walker, D., Gregory, F.M., Michelsen, A., Kumpula, T., Villoslada, M., Ylänne, H., Luoto, M., Virtanen, T., Forbes, B.C., Hölzel, N., Epstein, H., Heim, R.J., Bunn, A., Holmes, R.M., Hung, J.K.Y., Natali, S.M., Virkkala, A.-M., Goetz, S.J., 2024b. The Arctic Plant Aboveground Biomass Synthesis Dataset, Pan-Arctic, 1998–2022. Arct. Data Cent. https://doi.org/10.18739/A2RR1PP3N.

Bjorkman, A.D., García Criado, M., Myers-Smith, I.H., Ravolainen, V.T., Jónsdóttir, I.S., Westergaard, K.B., Lawler, J.P., Aronsson, M., Bennett, B., Gardfjell, H., Heiðmarsson, S., Stewart, L., Normand, S., 2020. Status and trends in Arctic vegetation: evidence from experimental warming and long-term monitoring. Ambio 49, 678–692. https://doi.org/10.1007/s13280-019-01161-6.

Blume-Werry, G., Wilson, S.D., Kreyling, J., Milbau, A., 2016. The hidden season: growing season is 50% longer below than above ground along an arctic elevation gradient. New Phytol. 209, 978–986. https://doi.org/10.1111/NPH.13655.

Breiman, L., 2001. Random forests. Mach. Learn. 45, 5–32. https://doi.org/10.1023/A:1010933404324/METRICS.

Brinkman, T.J., Hansen, W.D., Chapin, F.S., Kofinas, G., BurnSilver, S., Rupp, T.S., 2016. Arctic communities perceive climate impacts on access as a critical challenge to availability of subsistence resources. Clim. Chang. 139, 413–427. https://doi.org/10.1007/S10584-016-1819-6/TABLES/3.

Broecker, W.S., 1987. Unpleasant surprises in the greenhouse? Nat 3286126 (328), 123–126. https://doi.org/10.1038/328123a0.

Cahoon, S.M.P., Sullivan, P.F., Shaver, G.R., Welker, J.M., Post, E.S., 2012. Interactions among shrub cover and the soil microclimate may determine future Arctic carbon budgets. Ecol. Lett. 15, 1415–1422. https://doi.org/10.1111/j.1461-0248.2012.01865.x.

CAVM Team, 2003. Circumpolar Arctic vegetation map. In: Conservation of Arctic Flora and Fauna (CAFF) Map No. 1. U.S. Fish and Wildlife Service, Anchorage, Alaska.

Chapin, F.S., Fetcher, N., Kielland, K., Everett, K.R., Linkins, A.E., 1988. Productivity and nutrient cycling of Alaskan tundra: enhancement by flowing soil water. Ecology 69, 693–702. https://doi.org/10.2307/1941017.

Chapin, F.S., Sturm, M., Serreze, M.C., McFadden, J.P., Key, J.R., Lloyd, A.H., Mcguire, A.D., Rupp, T.S., Lynch, A.H., Schimel, J.P., Beringer, J., Chapman, W.L., Epstein, H.E., Euskirchen, E.S., Hinzman, L.D., Jia, G.J., Ping, C.L., Tape, K.D., Thompson, C.D.C., Walker, D.A., Welker, J.M., 2005. Role of land-surface changes in arctic summer warming. Science (80-.) 310, 657–660. https://doi.org/10.1126/science.1117368.

Chen, T., Guestrin, C., 2016. XGBoost: a scalable tree boosting system. In: Proc. ACM SIGKDD Int. Conf. Knowl. Discov. Data min. 13-17-August-2016, pp. 785–794. https://doi.org/10.1145/2939672.2939785.

Christen, P., Hand, D.J., 2023. A review of the F-measure: its history, properties, criticism, and alternatives. ACM Comput. Surv. 56. https://doi.org/10.1145/3606367.

Coops, N.C., Wulder, M.A., 2019. Breaking the habit(at). Trends Ecol. Evol. 34, 585–587. https://doi.org/10.1016/J.TREE.2019.04.013.

Cristianini, N., Shawe-Taylor, J., 2000. An introduction to support vector machines and other kernel-based learning methods. In: An Introd. to Support Vector Mach. Other Kernel-based Learn. Methods. https://doi.org/10.1017/CBO9780511801389.

Cuerrier, A., Brunet, N.D., Gérin-Lajoie, J., Downing, A., Lévesque, E., 2015. The study of Inuit knowledge of climate change in Nunavik, Quebec: a mixed methods approach. Hum. Ecol. 43, 379–394. https://doi.org/10.1007/S10745-015-9750-4/TABLES/5.

Cunliffe, A.M., Anderson, K., Boschetti, F., Brazier, R.E., Graham, H.A., Myers-Smith, I. H., Astor, T., Boer, M.M., Calvo, L.G., Clark, P.E., Cramer, M.D., Encinas-Lara, M.S., Escarzaga, S.M., Fernández-Guisuraga, J.M., Fisher, A.G., Gdulová, K., Gillespie, B. M., Griebel, A., Hanan, N.P., Hanggito, M.S., Haselberger, S., Havrilla, C.A., Heilman, P., Ji, W., Karl, J.W., Kirchhoff, M., Kraushaar, S., Lyons, M.B., Marzolff, I., Mauritz, M.E., McIntire, C.D., Metzen, D., Méndez-Barroso, L.A., Power, S.C., Prošek, J., Sanz-Ablanedo, E., Sauer, K.J., Schulze-Brüninghoff, D., Šímová, P., Sitch, S., Smit, J.L., Steele, C.M., Suárez-Seoane, S., Vargas, S.A., Villarreal, M.L., Visser, F., Wachendorf, M., Wirnsberger, H., Wojcikiewicz, R., 2022. Global Application of an Unoccupied Aerial Vehicle Photogrammetry Protocol for Predicting Aboveground Biomass in Non-forest Ecosystems. Ecol. Conserv, Remote Sens. https://doi.org/10.1002/RSE2.228.

Curasi, S.R., Loranty, M.M., Natali, S.M., 2016. Water track distribution and effects on carbon dioxide flux in an eastern Siberian upland tundra landscape. Environ. Res. Lett. 11, 045002. https://doi.org/10.1088/1748-9326/11/4/045002.

Cushman, S.A., Gutzweiler, K., Evans, J.S., McGarigal, K., 2010. The gradient paradigm: A conceptual and analytical framework for landscape ecology. In: Cushman, S.A., Huettmann, F. (Eds.), Spatial Complexity, Informatics, and Wildlife Conservation. Springer, Tokyo, Japan. https://doi.org/10.1007/978-4-431-87771-4_5.

DeMarco, J., Mack, M.C., Bret-Harte, M.S., 2014a. Effects of arctic shrub expansion on biophysical vs. biogeochemical drivers of litter decomposition. Ecology 95, 1861–1875. https://doi.org/10.1890/13-2221.1.

DeMarco, J., Mack, M.C., Bret-Harte, M.S., Burton, M., Shaver, G.R., 2014b. Long-term experimental warming and nutrient additions increase productivity in tall deciduous shrub tundra. Ecosphere 5, 1–22. https://doi.org/10.1890/ES13-00281.1.

Descals, A., Gaveau, D.L.A., Verger, A., Sheil, D., Naito, D., Peñuelas, J., 2022. Unprecedented fire activity above the Arctic circle linked to rising temperatures. Science (80-.) 378, 532–537. https://doi.org/10.1126/SCIENCE.ABN9768/SUPPL_FILE/SCIENCE.ABN9768_SM.PDF.

Dial, R.J., Maher, C.T., Hewitt, R.E., Sullivan, P.F., 2022. Sufficient conditions for rapid range expansion of a boreal conifer. Nat 608, 546–551. https://doi.org/10.1038/s41586-022-05093-2.

Dinerstein, E., Olson, D., Joshi, A., Vynne, C., Burgess, N.D., Wikramanayake, E., Hahn, N., Palminteri, S., Hedao, P., Noss, R., Hansen, M., Locke, H., Ellis, E.C., Jones, B., Barber, C.V., Hayes, R., Kormos, C., Martin, V., Crist, E., Sechrest, W., Price, L., Baillie, J.E.M., Weeden, D., Suckling, K., Davis, C., Sizer, N., Moore, R., Thau, D., Birch, T., Potapov, P., Turubanova, S., Tyukavina, A., De Souza, N., Pintea, L., Brito, J.C., Llewellyn, O.A., Miller, A.G., Patzelt, A., Ghazanfar, S.A., Timberlake, J., Klöser, H., Shennan-Farpón, Y., Kindt, R., Lillesø, J.P.B., Van Breugel, P., Graudal, L., Voge, M., Al-Shammari, K.F., Saleem, M., 2017. An ecoregion-based approach to protecting half the terrestrial realm. Bioscience 67, 534–545. https://doi.org/10.1093/BIOSCI/BIX014.

Ding, C., Peng, H., 2005. Minimum redundancy feature selection from microarray gene expression data. J. Bioinforma. Comput. Biol. 3, 185–205. https://doi.org/10.1142/S0219720005001004.

Duncanson, L., Disney, M., Armston, J., Nickeson, J., Minor, D., Camacho, F., 2021. Aboveground Woody biomass product validation good practices protocol, 1.0. Ed. In: Committee on Earth Observation Satellites: Working Group on Calibration and Validation land Product Validation Subgroup. https://doi.org/10.5067/doc/ceoswgcv/lpv/agb.001.

Duncanson, L., Montesano, P.M., Neuenschwander, A., Thomas, N., Mandel, A., Minor, D., Guenther, E., Hancock, S., Feng, T., Barciauskas, A., Chang, G.W., Shah, S., Satorius, B.P., 2023. Aboveground biomass density for high latitude forests from ICESat-2, 2020. In: ORNL DAAC, Oak Ridge, Tennessee, USA. https://doi.org/10.3334/ORNLDAAC/2186.

Elmendorf, S.C., Hollister, R.D., 2023. Limits on phenological response to high temperature in the Arctic. Sci. Report. 131 (13), 1–9. https://doi.org/10.1038/s41598-022-26955-9.

Elmendorf, S.C., Henry, G.H.R., Hollister, R.D., Björk, R.G., Boulanger-Lapointe, N., Cooper, E.J., Cornelissen, J.H.C., Day, T.A., Dorrepaal, E., Elumeeva, T.G., Gill, M., Gould, W.A., Harte, J., Hik, D.S., Hofgaard, A., Johnson, D.R., Johnstone, J.F., Jónsdóttir, I.S., Jorgenson, J.C., Klanderud, K., Klein, J.A., Koh, S., Kudo, G., Lara, M.J., Lévesque, E., Magnússon, B., May, J.L., Mercado-Díaz, J.A., Michelsen, A., Molau, U., Myers-Smith, I.H., Oberbauer, S.F., Onipchenko, V.G., Rixen, C., Schmidt, N.M., Shaver, G.R., Spasojevic, M.J., Þórhallsdóttir, Þ.E., Tolvanen, A., Troxler, T., Tweedie, C.E., Villareal, S., Wahren, C.-H., Walker, X.J., Webber, P.J., Welker, J.M., Wipf, S., 2012. Plot-scale evidence of tundra vegetation change and links to recent summer warming. Nat. Clim. Chang. 2, 453–457. https://doi.org/10.1038/nclimate1465.

Elvebakk, A., Elven, R., Razzhivin, V., 1999. Delimitation, zonal and sectorial subdivision of the Arctic for the Panarctic Flora project. In: Nordal, I., Razzhivin, V. (Eds.), The Species Concept in the High North — A Panarctic Flora Initiative. The Norwegian Academy of Science and Letters, Oslo, Norway, pp. 375–386.

Epstein, H.E., Raynolds, M.K., Walker, D.A., Bhatt, U.S., Tucker, C.J., Pinzon, J.E., 2012. Dynamics of aboveground phytomass of the circumpolar Arctic tundra during the past three decades. Environ. Res. Lett. 7, 015506. https://doi.org/10.1088/1748-9326/7/1/015506.

FAO, 2002. Second expert meeting on harmonizing Forest-related definitions for use by various stakeholders. In: Trines, E., Van Tol, G. (Eds.), Rome. Italy.

Fauchald, P., Park, T., Tømmervik, H., Myneni, R.B., Hausner, V.H., 2017. Arctic greening from warming promotes declines in caribou populations. Sci. Adv. 3, e1601365. https://doi.org/10.1126/sciadv.1601365.

Fisher, J.B., Hayes, D.J., Schwalm, C.R., Huntzinger, D.N., Stofferahn, E., Schaefer, K., Luo, Y., Wullschleger, S.D., Goetz, S., Miller, C.E., Griffith, P., Chadburn, S., Chatterjee, A., Ciais, P., Douglas, T.A., Genet, H., Ito, A., Neigh, C.S.R., Poulter, B., Rogers, B.M., Sonnentag, O., Tian, H., Wang, W., Xue, Y., Yang, Z.L., Zeng, N., Zhang, Z., 2018. Missing pieces to modeling the Arctic-boreal puzzle. Environ. Res. Lett. 13, 020202. https://doi.org/10.1088/1748-9326/AA9D9A.

Foga, S., Scaramuzza, P.L., Guo, S., Zhu, Z., Dilley, R.D., Beckmann, T., Schmidt, G.L., Dwyer, J.L., Joseph Hughes, M., Laue, B., 2017. Cloud detection algorithm comparison and validation for operational Landsat data products. Remote Sens. Environ. 194, 379–390. https://doi.org/10.1016/J.RSE.2017.03.026.

Forbes, B.C., Stammler, F., Kumpula, T., Meschtyb, N., Pajunen, A., Kaarlejärvi, E., 2009. High resilience in the Yamal-Nenets social-ecological system, west Siberian Arctic, Russia. Proc. Natl. Acad. Sci. USA 106, 22041–22048. https://doi.org/10.1073/PNAS.0908286106/SUPPL_FILE/0908286106SI.PDF.

Foster, A.C., Wang, J.A., Frost, G.V., Davidson, S.J., Hoy, E., Turner, K.W., Sonnentag, O., Epstein, H., Berner, L.T., Armstrong, A.H., Kang, M., Rogers, B.M., Campbell, E., Miner, K.R., Orndahl, K.M., Bourgeau-Chavez, L.L., Lutz, D.A., French, N., Chen, D., Du, J., Shestakova, T.A., Shuman, J.K., Tape, K., Virkkala, A.M., Potter, C., Goetz, S., 2022. Disturbances in north American boreal forest and Arctic tundra: impacts, interactions, and responses. Environ. Res. Lett. 17, 113001. https://doi.org/10.1088/1748-9326/AC98D7.

Frost, G.V., Epstein, H.E., Walker, D.A., 2014. Regional and landscape-scale variability of Landsat-observed vegetation dynamics in northwest Siberian tundra. Environ. Res. Lett. 9, 025004. https://doi.org/10.1088/1748-9326/9/2/025004.

Gaglioti, B.V., Berner, L.T., Jones, B.M., Orndahl, K.M., Williams, A.P., Andreu-Hayles, L., D'Arrigo, R.D., Goetz, S.J., Mann, D.H., 2021. Tussocks enduring or shrubs greening: alternate responses to changing fire regimes in the Noatak River valley, Alaska. J. Geophys. Res. Biogeosci. 126, e2020JG006009. https://doi.org/10.1029/2020JG006009.

Gaspard, A., Boudreau, S., 2024. Climate predicts NDVI better than Plant functional group attributes along a latitudinal gradient in Nunavik. J. Biogeogr. 0, 1–13. https://doi.org/10.1111/JBI.15024.

Gauthier, G., Bêty, J., Cadieux, M.C., Legagneux, P., Doiron, M., Chevallier, C., Lai, S., Tarroux, A., Berteaux, D., 2013. Long-term monitoring at multiple trophic levels suggests heterogeneity in responses to climate change in the Canadian Arctic tundra. Philos. Trans. R. Soc. B Biol. Sci. 368. https://doi.org/10.1098/RSTB.2012.0482.

Google Earth 9.194.0.0 [WWW Document]. URL. https://earth.google.com/web/.

Gorelick, N., Hancher, M., Dixon, M., Ilyushchenko, S., Thau, D., Moore, R., 2017. Google earth engine: planetary-scale geospatial analysis for everyone. Remote Sens. Environ. 202, 18–27. https://doi.org/10.1016/j.rse.2017.06.031.

Hand, D.J., Till, R.J., 2001. A simple generalisation of the area under the ROC curve for multiple class classification problems. Mach. Learn. 45, 171–186. https://doi.org/10.1023/A:1010920819831/METRICS.

Hawksworth, D.L., Grube, M., 2020. Lichens redefined as complex ecosystems. New Phytol. 227, 1281. https://doi.org/10.1111/NPH.16630.

Heijmans, M.M.P.D., Magnússon, R., Lara, M.J., Frost, G.V., Myers-Smith, I.H., van Huissteden, J., Jorgenson, M.T., Fedorov, A.N., Epstein, H.E., Lawrence, D.M., Limpens, J., 2022. Tundra vegetation change and impacts on permafrost. Nat. Rev. Earth Environ. 31 (3), 68–84. https://doi.org/10.1038/s43017-021-00233-0.

Howat, I., 2017. MEaSUREs Greenland ice mapping project (GIMP) land ice and ocean classification mask, version 1. In: NASA National Snow and Ice Data Center Distributed Active Archive Center. Boulder, Colorado USA. https://doi.org/10.5067/B8X58MQBFUPA.

Howat, I.M., Negrete, A., Smith, B.E., 2014. The Greenland ice mapping project (GIMP) land classification and surface elevation data sets. Cryosphere 8, 1509–1518. https://doi.org/10.5194/TC-8-1509-2014.

Hu, F.S., Higuera, P.E., Duffy, P.A., Chipman, M.L., Rocha, A.V., Young, A.M., Kelly, R., Dietze, M.C., 2015. Arctic tundra fires: natural variability and responses to climate change. Front. Ecol. Environ. 13, 369–377. https://doi.org/10.1890/150063.

Iversen, C.M., Sloan, V.L., Sullivan, P.F., Euskirchen, E.S., Mcguire, A.D., Norby, R.J., Walker, A.P., Warren, J.M., Wullschleger, S.D., 2015. The unseen iceberg: plant roots in arctic tundra. New Phytol. 205, 34–58. https://doi.org/10.1111/NPH.13003.

Jackson, R.B., Canadell, J., Ehleringer, J.R., Mooney, H.A., Sala, O.E., Schulze, E.D., 1996. A global analysis of root distributions for terrestrial biomes. Oecologia 108, 389–411. https://doi.org/10.1007/BF00333714/METRICS.

Johansen, B., Tømmervik, H., 2014. The relationship between phytomass, NDVI and vegetation communities on Svalbard. Int. J. Appl. Earth Obs. Geoinf. 27, 20–30. https://doi.org/10.1016/J.JAG.2013.07.001.

Jones, B.M., Breen, A.L., Gaglioti, B.V., Mann, D.H., Rocha, A.V., Grosse, G., Arp, C.D., Kunz, M.L., Walker, D.A., 2013. Identification of unrecognized tundra fire events on the north slope of Alaska. J. Geophys. Res. Biogeosci. 118, 1334–1344. https://doi.org/10.1002/jgrg.20113.

Jorgenson, M.T., Shur, Y.L., Pullman, E.R., 2006. Abrupt increase in permafrost degradation in Arctic Alaska. Geophys. Res. Lett. 33, 2–5. https://doi.org/10.1029/2005GL024960.

Karger, D.N., Conrad, O., Böhner, J., Kawohl, T., Kreft, H., Soria-Auza, R.W., Zimmermann, N.E., Linder, H.P., Kessler, M., 2017. Climatologies at high resolution for the earth's land surface areas. Sci. Data 4. https://doi.org/10.1038/SDATA.2017.122.

Karger, D.N., Conrad, O., Böhner, J., Kawohl, T., Kreft, H., Soria-Auza, R.W., Zimmermann, N.E., Linder, H.P., Kessler, M., 2018. Climatologies at High Resolution for the earth's Land Surface Areas [Dataset]. https://doi.org/10.5061/dryad.kd1d4.

Ke, G., Meng, Q., Finley, T., Wang, T., Chen, W., Ma, W., Ye, Q., Liu, T.-Y., 2017. LightGBM: A Highly Efficient Gradient Boosting Decision Tree. Adv. Neural Inf. Proces. Syst. 30.

Kharuk, V.I., Petrov, I.A., Krivobokov, L.V., Golyukov, A.S., Dvinskaya, M.L., Im, S.T., Shushpanov, A.S., Smith, K.T., 2023. Larch response to warming in northern Siberia. Reg. Environ. Chang. 23, 1–12. https://doi.org/10.1007/S10113-022-02016-9/METRICS.

Kokelj, S.V., Lacelle, D., Lantz, T.C., Tunnicliffe, J., Malone, L., Clark, I.D., Chin, K.S., 2013. Thawing of massive ground ice in mega slumps drives increases in stream sediment and solute flux across a range of watershed scales. Case Rep. Med. 118, 681–692. https://doi.org/10.1002/JGRF.20063.

Kuhn, M., Wickham, H., 2022. Tidymodels: a collection of packages for modeling and machine learning using tidyverse principles.

Lamarque, L.J., Félix-Faure, J., Deschamps, L., Lévesque, E., Cusson, P.O., Fortier, D., Giacomazzo, M., Guillemette, F., Paillassa, J., Tremblay, M., Maire, V., 2023. Hydrological regime and plant functional traits jointly mediate the influence of Salix spp. on soil organic carbon stocks in a high Arctic tundra. Ecosystems 26, 1238–1259. https://doi.org/10.1007/S10021-023-00829-1/FIGURES/6.

Lantz, T.C., Kokelj, S.V., Gergel, S.E., Henry, G.H.R., 2009. Relative impacts of disturbance and temperature: persistent changes in microenvironment and

vegetation in retrogressive thaw slumps. Glob. Chang. Biol. 15, 1664–1675. https://doi.org/10.1111/j.1365-2486.2009.01917.x.
Lara, M.J., McGuire, A.D., Euskirchen, E.S., Genet, H., Yi, S., Rutter, R., Iversen, C., Sloan, V., Wullschleger, S.D., 2020. Local-scale Arctic tundra heterogeneity affects regional-scale carbon dynamics. Nat. Commun. 111 (11), 1–10. https://doi.org/10.1038/s41467-020-18768-z.
Legendre, P., Dale, M.R.T., Fortin, M.-J., Gurevitch, J., Hohn, M., Legendre, D.M., Dale, P., Fortin, M.R.T., Gurevitch, M.-J., Hohn, J., Myers, M., Fortin, M.-J., 2002. The consequences of spatial structure for the design and analysis of ecological field surveys. Ecography (Cop.). 25, 601–615. https://doi.org/10.1034/J.1600-0587.2002.250508.X.
Lewkowicz, A.G., Way, R.G., 2019. Extremes of summer climate trigger thousands of thermokarst landslides in a high Arctic environment. Nat. Commun. 101 (10), 1–11. https://doi.org/10.1038/s41467-019-09314-7.
Loranty, M.M., Goetz, S.J., Beck, P.S.A., 2011. Tundra vegetation effects on pan-Arctic albedo. Environ. Res. Lett. 6, 024014. https://doi.org/10.1088/1748-9326/6/2/024014.
Macander, M.J., Nelson, P.R., Nawrocki, T.W., Frost, G.V., Orndahl, K.M., Palm, E.C., Wells, A.F., Goetz, S.J., 2022. Time-series maps reveal widespread change in plant functional type cover across arctic and boreal Alaska and Yukon. Environ. Res. Lett. https://doi.org/10.1088/1748-9326/AC6965.
Matasci, G., Hermosilla, T., Wulder, M.A., White, J.C., Coops, N.C., Hobart, G.W., Zald, H.S.J., 2018. Large-area mapping of Canadian boreal forest cover, height, biomass and other structural attributes using Landsat composites and lidar plots. Remote Sens. Environ. 209, 90–106. https://doi.org/10.1016/J.RSE.2017.12.020.
McKay, M.D., Beckman, R.J., Conover, W.J., 1979. A comparison of three methods for selecting values of input variables in the analysis of output from a computer code. Technometrics 21, 239. https://doi.org/10.2307/1268522.
Mekonnen, Z.A., Riley, W.J., Grant, R.F., 2018. Accelerated nutrient cycling and increased light competition will Lead to 21st century shrub expansion in north American Arctic tundra. J. Geophys. Res. Biogeosci. 123, 1683–1701. https://doi.org/10.1029/2017JG004319.
Mekonnen, Z.A., Riley, W.J., Berner, L.T., Bouskill, N.J., Torn, M.S., Iwahana, G., Breen, A.L., Myers-Smith, I.H., Criado, M.G., Liu, Y., Euskirchen, E.S., Goetz, S.J., Mack, M.C., Grant, R.F., 2021. Arctic tundra shrubification: a review of mechanisms and impacts on ecosystem carbon balance. Environ. Res. Lett. 16, 053001. https://doi.org/10.1088/1748-9326/ABF28B.
Meta, World Resources Institute, 2023. High Resolution Canopy Height Maps (CHM). Google Earth Engine.
Metcalfe, D.B., Hermans, T.D.G., Ahlstrand, J., Becker, M., Berggren, M., Björk, R.G., Björkman, M.P., Blok, D., Chaudhary, N., Chisholm, C., Classen, A.T., Hasselquist, N. J., Jonsson, M., Kristensen, J.A., Kumordzi, B.B., Lee, H., Mayor, J.R., Prevéy, J., Pantazatou, K., Rousk, J., Sponseller, R.A., Sundqvist, M.K., Tang, J., Uddling, J., Wallin, G., Zhang, W., Ahlström, A., Tenenbaum, D.E., Abdi, A.M., 2018. Patchy field sampling biases understanding of climate change impacts across the Arctic. Nat. Ecol. Evol. 29 (2), 1443–1448. https://doi.org/10.1038/s41559-018-0612-5.
Mokany, K., Raison, R.J., Prokushkin, A.S., 2006. Critical analysis of root : shoot ratios in terrestrial biomes. Glob. Chang. Biol. 12, 84–96. https://doi.org/10.1111/J.1365-2486.2005.001043.X.
Moreira, E.P., Valeriano, M.M., 2014. Application and evaluation of topographic correction methods to improve land cover mapping using object-based classification. Int. J. Appl. Earth Obs. Geoinf. 32, 208–217. https://doi.org/10.1016/J.JAG.2014.04.006.
Myers-Smith, I.H., Elmendorf, S.C., Beck, P.S.A., Wilmking, M., Hallinger, M., Blok, D., Tape, K.D., Rayback, S.A., Macias-Fauria, M., Forbes, B.C., Speed, J.D.M., Boulanger-Lapointe, N., Rixen, C., Lévesque, E., Schmidt, N.M., Baittinger, C., Trant, A.J., Hermanutz, L., Collier, L.S., Dawes, M.A., Lantz, T.C., Weijers, S., JØrgensen, R.H., Buchwal, A., Buras, A., Naito, A.T., Ravolainen, V., Schaepman-Strub, G., Wheeler, J. A., Wipf, S., Guay, K.C., Hik, D.S., Vellend, M., 2015. Climate sensitivity of shrub growth across the tundra biome. Nat. Clim. Chang. 59 (5), 887–891. https://doi.org/10.1038/nclimate2697.
Myers-Smith, I.H., Grabowski, M.M., Thomas, H.J.D., Angers-Blondin, S., Daskalova, G. N., Bjorkman, A.D., Cunliffe, A.M., Assmann, J.J., Boyle, J.S., McLeod, E., McLeod, S., Joe, R., Lennie, P., Arey, D., Gordon, R.R., Eckert, C.D., 2019. Eighteen years of ecological monitoring reveals multiple lines of evidence for tundra vegetation change. Ecol. Monogr. e01351. https://doi.org/10.1002/ecm.1351.
Myers-Smith, I.H., Kerby, J.T., Phoenix, G.K., Bjerke, J.W., Epstein, H.E., Assmann, J.J., John, C., Andreu-Hayles, L., Angers-Blondin, S., Beck, P.S.A., Berner, L.T., Bhatt, U. S., Bjorkman, A.D., Blok, D., Bryn, A., Christiansen, C.T., Cornelissen, J.H.C., Cunliffe, A.M., Elmendorf, S.C., Forbes, B.C., Goetz, S.J., Hollister, R.D., de Jong, R., Loranty, M.M., Macias-Fauria, M., Maseyk, K., Normand, S., Olofsson, J., Parker, T. C., Parmentier, F.J.W., Post, E.S., Schaepman-Strub, G., Stordal, F., Sullivan, P.F., Thomas, H.J.D., Tømmervik, H., Treharne, R., Tweedie, C.E., Walker, D.A., Wilmking, M., Wipf, S., 2020. Complexity Revealed in the Greening of the Arctic. Nat. Clim. Chang. https://doi.org/10.1038/s41558-019-0688-1.
Myneni, R.B., Keeling, C.D., Tucker, C.J., Asrar, G., Nemani, R.R., 1997. Increased plant growth in the northern high latitudes from 1981 to 1991. Nat 386, 698–702. https://doi.org/10.1038/386698a0.
Naito, A.T., Cairns, D.M., 2011. Relationships between Arctic shrub dynamics and topographically derived hydrologiccharacteristics. Environ. Res. Lett. 6, 045506. https://doi.org/10.1088/1748-9326/6/4/045506.
Nelson, P.R., Maguire, A.J., Pierrat, Z., Orcutt, E.L., Yang, D., Serbin, S.P., Frost, G.V., Macander, M.J., Magney, T.S., Thompson, D.R., Wang, J.A., Oberbauer, S.F., Zesati, S.V., Davidson, S.J., Epstein, H.E., Unger, S., Campbell, P.K.E., Carmon, N., Velez-Reyes, M., Huemmrich, K.F., 2022. Remote sensing of tundra ecosystems using high spectral resolution reflectance: opportunities and challenges. J. Geophys. Res. Biogeosci. 127, e2021JG006697. https://doi.org/10.1029/2021JG006697.
Nitze, I., Heidler, K., Barth, S., Grosse, G., 2021. Developing and testing a deep learning approach formapping retrogressive thaw slumps. Remote Sens. 13, 4294. https://doi.org/10.3390/RS13214294/S1.
Orndahl, K.M.. https://doi.org/10.5281/zenodo.15059170.
Orndahl, K.M., Burns, P., 2024. rf_r_to_gee. https://doi.org/10.5281/ZENODO.13871352.
Orndahl, K.M., Berner, L.T., Rose, M., Arndal, M.F., Alexander, H.D., Yang, D., Humphreys, E.R., Loranty, M.M., Ludwig, S.M., Nyman, J., Juutinen, S., Aurela, M., Mikola, J., Mack, M.C., Vankoughnett, M.R., Iversen, C.M., Salmon, V.G., Kumar, J., Grogan, P., Danby, R.K., Scott, N.A., Olofsson, J., Siewert, M.B., Deschamps, L., Lévesque, E., Maire, V., Gauthier, G., Boudreau, S., Gaspard, A., Bret-Harte, M.S., Greaves, H.E., Walker, D., Michelsen, A., Kumpula, T., Villoslada, M., Ylänne, H., Luoto, M., Virtanen, T., Forbes, B.C., Hölzel, N., Epstein, H., Heim, R.J., Bunn, A., Holmes, R.M., Natali, S.M., Virkkala, A.-M., Goetz, S.J., (2024). Gridded 30-meter resolution estimates of aboveground plant biomass, woody plant biomass and woody plant dominance across the Arctic tundra biome (2020)., Arct. Data Cent.
Orndahl, K.M., Ehlers, L.P.W., Herriges, J.D., Pernick, R.E., Hebblewhite, M., Goetz, S.J., 2022a. Mapping Tundra Ecosystem Plant Functional Type Cover, Height and Aboveground Biomass in Alaska and Northwest Canada Using Unmanned Aerial Vehicles. Arct. Sci. 8, 1165–1180. https://cdnsciencepub.com/doi/pdf/10.1139/AS-2021-0044.
Orndahl, K.M., Macander, M.J., Berner, L.T., Goetz, S.J., 2022b. Plant functional type aboveground biomass change within Alaska and Northwest Canada mapped using a 35-year satellite time series from 1985 to 2020. Environ. Res. Lett. 17, 115010. https://doi.org/10.1088/1748-9326/AC9D50.
Open Source Geospatial Foundation Project, 2024. QGIS Geographic Information System.
Paustian, K., Ravindranath, N.H., van Amstel, A.R., 2006. 2006 IPCC Guidelines for National Greenhouse gas Inventories.
Pearson, R.G., Phillips, S.J., Loranty, M.M., Beck, P.S.A., Damoulas, T., Knight, S.J., Goetz, S.J., 2013. Shifts in Arctic vegetation and associated feedbacks under climate change. Nat. Clim. Chang. 3, 673–677. https://doi.org/10.1038/nclimate1858.
Pekel, J.-F., Cottam, A., Gorelick, N., Belward, A.S., 2016. High-resolution mapping of global surface water and its long-term changes. Nature 540, 418–422. https://doi.org/10.1038/nature20584.
Piao, S., Nan, H., Huntingford, C., Ciais, P., Friedlingstein, P., Sitch, S., Peng, S., Ahlström, A., Canadell, J.G., Cong, N., Levis, S., Levy, P.E., Liu, L., Lomas, M.R., Mao, J., Myneni, R.B., Peylin, P., Poulter, B., Shi, X., Yin, G., Viovy, N., Wang, T., Wang, X., Zaehle, S., Zeng, N., Zeng, Z., Chen, A., 2014. Evidence for a weakening relationship between interannual temperature variability and northern vegetation activity. Nat. Commun. 51 (5), 1–7. https://doi.org/10.1038/ncomms6018.
Poggio, L., De Sousa, L.M., Batjes, N.H., Heuvelink, G.B.M., Kempen, B., Ribeiro, E., Rossiter, D., 2021. SoilGrids 2.0: producing soil information for the globe with quantified spatial uncertainty. SOIL 7, 217–240. https://doi.org/10.5194/SOIL-7-217-2021.
R Core Team, 2020. R: A language and environment for statistical computing.
Rantanen, M., Karpechko, A.Y., Lipponen, A., Nordling, K., Hyvärinen, O., Ruosteenoja, K., Vihma, T., Laaksonen, A., 2022. The Arctic has warmed nearly four times faster than the globe since 1979. Commun. Earth Environ. 31 (3), 1–10. https://doi.org/10.1038/s43247-022-00498-3.
Räsänen, A., Juutinen, S., Aurela, M., Virtanen, T., 2018. Predicting aboveground biomass in Arctic landscapes using very high spatial resolution satellite imagery and field sampling. Int. J. Remote Sens. 40, 1175–1199. https://doi.org/10.1080/01431161.2018.1524176.
Raynolds, M.K., Walker, D.A., 2009. Effects of deglaciation on circumpolar distribution of arctic vegetation. Can. J. Remote. Sens. 35, 118–129. https://doi.org/10.5589/M09-006.
Raynolds, M.K., Walker, D.A., Epstein, H.E., Pinzon, J.E., Tucker, C.J., 2012. A new estimate of tundra-biome phytomass from trans-Arctic field data and AVHRR NDVI. Remote Sens. Lett. 3, 403–411. https://doi.org/10.1080/01431161.2011.609188.
Raynolds, M.K., Walker, D.A., Balser, A., Bay, C., Campbell, M., Cherosov, M.M., Daniëls, F.J.A., Eidesen, P.B., Ermokhina, K.A., Frost, G.V., Jedrzejek, B., Jorgenson, M.T., Kennedy, B.E., Kholod, S.S., Lavrinenko, I.A., Lavrinenko, O.V., Magnússon, B., Matveyeva, N.V., Metúsalemsson, S., Nilsen, L., Olthof, I., Pospelov, I.N., Pospelova, E.B., Pouliot, D., Razzhivin, V., Schaepman-Strub, G., Šibík, J., Telyatnikov, M.Y., Troeva, E., 2019. A raster version of the circumpolar Arctic vegetation map (CAVM). Remote Sens. Environ. 232, 111297. https://doi.org/10.1016/J.RSE.2019.111297.
Rickbeil, G.J.M., Hermosilla, T., Coops, N.C., White, J.C., Wulder, M.A., Lantz, T.C., 2018. Changing northern vegetation conditions are influencing barren ground caribou (Rangifer tarandus groenlandicus) post-calving movement rates. J. Biogeogr. 45, 702–712. https://doi.org/10.1111/jbi.13161.
Riihimäki, H., Luoto, M., Heiskanen, J., 2019. Estimating fractional cover of tundra vegetation at multiple scales using unmanned aerial systems and optical satellite data. Remote Sens. Environ. 224, 119–132. https://doi.org/10.1016/j.rse.2019.01.030.
Riley, W.J., Mekonnen, Z.A., Tang, J., Zhu, Q., Bouskill, N.J., Grant, R.F., 2021. Non-growing season plant nutrient uptake controls Arctic tundra vegetation composition under future climate. Environ. Res. Lett. 16, 074047. https://doi.org/10.1088/1748-9326/AC0E63.
Schuur, E.A.G., Abbott, B.W., Commane, R., Ernakovich, J., Euskirchen, E., Hugelius, G., Grosse, G., Jones, M., Koven, C., Leshyk, V., Lawrence, D., Loranty, M.M., Mauritz, M., Olefeldt, D., Natali, S., Rodenhizer, H., Salmon, V., Schädel, C., Strauss, J., Treat, C., Turetsky, M., 2022. Permafrost and climate change: carbon

cycle feedbacks from the warming Arctic. Annu. Rev. Environ. Resour. 47, 343–371. https://doi.org/10.1146/ANNUREV-ENVIRON-012220-011847/1.
Serreze, M.C., Barry, R.G., 2011. Processes and impacts of Arctic amplification: a research synthesis. Glob. Planet. Chang. 77, 85–96. https://doi.org/10.1016/J.GLOPLACHA.2011.03.004.
Shaver, G.R., Chapin, F.S., 1991. Production: biomass relationships and element cycling in contrasting Arctic vegetation types. Ecol. Monogr. 61, 1–31. https://doi.org/10.2307/1942997.
Siewert, M.B., Olofsson, J., 2020. Scale-dependency of Arctic ecosystem properties revealed by UAV. Environ. Res. Lett. 15, 129601. https://doi.org/10.1088/1748-9326/aba20b.
Siewert, M.B., Hanisch, J., Weiss, N., Kuhry, P., Maximov, T.C., Hugelius, G., 2015. Comparing carbon storage of Siberian tundra and taiga permafrost ecosystems at very high spatial resolution. J. Geophys. Res. Biogeosci. 120, 1973–1994. https://doi.org/10.1002/2015JG002999.
Skarin, A., Verdonen, M., Kumpula, T., MacIas-Fauria, M., Alam, M., Kerby, J., Forbes, B. C., 2020. Reindeer use of low Arctic tundra correlates with landscape structure. Environ. Res. Lett. 15, 115012. https://doi.org/10.1088/1748-9326/ABBF15.
Soenen, S.A., Peddle, D.R., Coburn, C.A., 2005. SCS+C: a modified sun-canopy-sensor topographic correction in forested terrain. IEEE Trans. Geosci. Remote Sens. 43, 2148–2159. https://doi.org/10.1109/TGRS.2005.852480.
Sola, I., González-Audícana, M., Álvarez-Mozos, J., 2016. Multi-criteria evaluation of topographic correction methods. Remote Sens. Environ. 184, 247–262. https://doi.org/10.1016/J.RSE.2016.07.002.
Spawn, S.A., Gibbs, H.K., 2020. Global aboveground and belowground biomass carbon density maps for the year 2010. In: ORNL DAAC, Oak Ridge, Tennessee, USA. https://doi.org/10.3334/ORNLDAAC/1763.
Spawn, S.A., Sullivan, C.C., Lark, T.J., Gibbs, H.K., 2020. Harmonized global maps of above and belowground biomass carbon density in the year 2010. Sci. Data 7, 1–22. https://doi.org/10.1038/s41597-020-0444-4.
Sturm, M., 2005. Changing snow and shrub conditions affect albedo with global implications. J. Geophys. Res. 110, G01004. https://doi.org/10.1029/2005JG000013.
Sturm, M., Mcfadden, J.P., Liston, G.E., Stuart Chapin Iii, F., Racine, C.H., Holmgren, J., 2001. Snow–Shrub Interactions in Arctic Tundra: A Hypothesis with Climatic Implications. J. Clim. 14, 336–344. https://doi.org/10.1175/1520-0442(2001)014.
Sulman, B.N., Salmon, V.G., Iversen, C.M., Breen, A.L., Yuan, F., Thornton, P.E., 2021. Integrating Arctic plant functional types in a land surface model using above- and belowground field observations. J. Adv. Model. Earth Syst. 13, e2020MS002396. https://doi.org/10.1029/2020MS002396.
Sweet, S.K., Asmus, A., Rich, M.E., Wingfield, J., Gough, L., Boelman, N.T., 2015. NDVI as a predictor of canopy arthropod biomass in the Alaskan arctic tundra. Ecol. Appl. 25, 779–790. https://doi.org/10.1890/14-0632.1.
Tape, K.D., Hallinger, M., Welker, J.M., Ruess, R.W., 2012. Landscape heterogeneity of shrub expansion in Arctic Alaska. Ecosystems 15, 711–724. https://doi.org/10.1007/s10021-012-9540-4.
Tape, K.D., Gustine, D.D., Ruess, R.W., Adams, L.G., Clark, J.A., 2016. Range expansion of moose in Arctic Alaska linked to warming and increased shrub habitat. PLoS One 11, e0152636. https://doi.org/10.1371/JOURNAL.PONE.0152636.
Tape, K.D., Jones, B.M., Arp, C.D., Nitze, I., Grosse, G., 2018. Tundra be dammed: beaver colonization of the Arctic. Glob. Chang. Biol. 24, 4478–4488. https://doi.org/10.1111/GCB.14332.
Tolan, J., Yang, H.I., Nosarzewski, B., Couairon, G., Vo, H.V., Brandt, J., Spore, J., Majumdar, S., Haziza, D., Vamaraju, J., Moutakanni, T., Bojanowski, P., Johns, T., White, B., Tiecke, T., Couprie, C., 2024. Very high resolution canopy height maps from RGB imagery using self-supervised vision transformer and convolutional decoder trained on aerial lidar. Remote Sens. Environ. 300. https://doi.org/10.1016/j.rse.2023.113888.
Tucker, C.J., Sellers, P.J., 1986. Satellite remote sensing of primary production. Int. J. Remote Sens. 7, 1395–1416. https://doi.org/10.1080/01431168608948944.
Villoslada, M., Berner, L.T., Juutinen, S., Ylänne, H., Kumpula, T., 2024. Upscaling vascular aboveground biomass and topsoil moisture of subarctic fens from unoccupied aerial vehicles (UAVs) to satellite level. Sci. Total Environ. 933, 173049. https://doi.org/10.1016/J.SCITOTENV.2024.173049.
Virkkala, A.-M., Abdi, A.M., Luoto, M., Metcalfe, D.B., 2019. Identifying multidisciplinary research gaps across Arctic terrestrial gradients. Environ. Res. Lett. 14, 124061. https://doi.org/10.1088/1748-9326/AB4291.
Virkkala, A.M., Aalto, J., Rogers, B.M., Tagesson, T., Treat, C.C., Natali, S.M., Watts, J.D., Potter, S., Lehtonen, A., Mauritz, M., Schuur, E.A.G., Kochendorfer, J., Zona, D., Oechel, W., Kobayashi, H., Humphreys, E., Goeckede, M., Iwata, H., Lafleur, P.M., Euskirchen, E.S., Bokhorst, S., Marushchak, M., Martikainen, P.J., Elberling, B., Voigt, C., Biasi, C., Sonnentag, O., Parmentier, F.J.W., Ueyama, M., Celis, G., St Louis, V.L., Emmerton, C.A., Peichl, M., Chi, J., Järveoja, J., Nilsson, M.B., Oberbauer, S.F., Torn, M.S., Park, S.J., Dolman, H., Mammarella, I., Chae, N., Poyatos, R., López-Blanco, E., Christensen, T.R., Kwon, M.J., Sachs, T., Holl, D., Luoto, M., 2021. Statistical upscaling of ecosystem CO2 fluxes across the terrestrial tundra and boreal domain: regional patterns and uncertainties. Glob. Chang. Biol. 27, 4040–4059. https://doi.org/10.1111/GCB.15659.
Virtanen, R., Oksanen, L., Oksanen, T., Cohen, J., Forbes, B.C., Johansen, B., K€ Ayhk€, O.J., Olofsson, J., Pulliainen, J., Tømmervik, H., 2016. Where do the treeless tundra areas of northern highlands fit in the global biome system: toward an ecologically natural subdivision of the tundra biome. Ecol. Evol. 6, 143–158. https://doi.org/10.1002/ece3.1837.
Walker, D.A., Raynolds, M.K., Daniëls, F.J.A., Einarsson, E., Elvebakk, A., Gould, W.A., Katenin, A.E., Kholod, S.S., Markon, C.J., Melnikov, E.S., Moskalenko, N.G., Talbot, S.S., Yurtsev, B.A., 2005. The circumpolar Arctic vegetation map. J. Veg. Sci. 16, 267–282. https://doi.org/10.1111/j.1654-1103.2005.tb02365.x.
Walker, D.A., Epstein, H.E., Romanovsky, V.E., Ping, C.L., Michaelson, G.J., Daanen, R. P., Shur, Y., Peterson, R.A., Krantz, W.B., Raynolds, M.K., Gould, W.A., Gonzalez, G., Nicolsky, D.J., Vonlanthen, C.M., Kade, A.N., Kuss, P., Kelley, A.M., Munger, C.A., Tarnocai, C.T., Matveyeva, N.V., Daniëls, F.J.A., 2008. Arctic patterned-ground ecosystems: a synthesis of field studies and models along a north American Arctic transect. J. Geophys. Res. Biogeosci. 113. https://doi.org/10.1029/2007JG000504.
Walker, D.A., Epstein, H.E., Raynolds, M.K., Kuss, P., Kopecky, M.A., Frost, G.V., Daniëls, F.J.A., Leibman, M.O., Moskalenko, N.G., Matyshak, G.V., Khitun, O.V., Khomutov, A.V., Forbes, B.C., Bhatt, U.S., Kade, A.N., Vonlanthen, C.M., Tichý, L., 2012. Environment, vegetation and greenness (NDVI) along the North America and Eurasia Arctic transects. Environ. Res. Lett. 7, 015504. https://doi.org/10.1088/1748-9326/7/1/015504.
Wang, P., Heijmans, M.M.P.D., Mommer, L., van Ruijven, J., Maximov, T.C., Berendse, F., 2016. Belowground plant biomass allocation in tundra ecosystems and its relationship with temperature. Environ. Res. Lett. 11, 55003. https://doi.org/10.1088/1748-9326/11/5/055003.
Wang, J.A., Baccini, A., Farina, M., Randerson, J.T., Friedl, M.A., 2021. Disturbance suppresses the aboveground carbon sink in north American boreal forests. Nat. Clim. Chang. 115 (11), 435–441. https://doi.org/10.1038/s41558-021-01027-4.
Wulder, M.A., White, J.C., Loveland, T.R., Woodcock, C.E., Belward, A.S., Cohen, W.B., Fosnight, E.A., Shaw, J., Masek, J.G., Roy, D.P., 2016. The global Landsat archive: status, consolidation, and direction. Remote Sens. Environ. 185, 271–283. https://doi.org/10.1016/J.RSE.2015.11.032.
Yamazaki, D., Ikeshima, D., Sosa, J., Bates, P.D., Allen, G.H., Pavelsky, T.M., 2019. MERIT hydro: a high-resolution global hydrography map based on latest topography dataset. Water Resour. Res. 55, 5053–5073. https://doi.org/10.1029/2019WR024873.
Yin, G., Li, A., Wu, S., Fan, W., Zeng, Y., Yan, K., Xu, B., Li, J., Liu, Q., 2018. PLC: a simple and semi-physical topographic correction method for vegetation canopies based on path length correction. Remote Sens. Environ. 215, 184–198. https://doi.org/10.1016/J.RSE.2018.06.009.
Youden, W.J., 1950. Index for rating diagnostic tests. Cancer. https://doi.org/10.1002/1097-0142.
Yu, Q., Epstein, H.E., Engstrom, R., Walker, D.A., 2017. Circumpolar arctic tundra biomass and productivity dynamics in response to projected climate change and herbivory. Glob. Chang. Biol. 23, 3895–3907. https://doi.org/10.1111/gcb.13632.
Zanaga, D., Van De Kerchove, R., Daems, D., De Keersmaecker .B., W.C., Kirches, G., Wevers, J., Cartus, O., Santoro, M., Fritz, S., Lesiv, M., Herold, M., Tsendbazar, N.E., Xu, P., Ramoino, F., Arino, O., 2022. ESA WorldCover 10 m 2021 v200. https://doi.org/10.5281/zenodo.7254221.
Zhou, J., Tape, K.D., Prugh, L., Kofinas, G., Carroll, G., Kielland, K., 2020. Enhanced shrub growth in the Arctic increases habitat connectivity for browsing herbivores. Glob. Chang. Biol. 26, 3809–3820. https://doi.org/10.1111/GCB.15104.
Zhu, Z., Woodcock, C.E., 2014. Continuous change detection and classification of land cover using all available Landsat data. Remote Sens. Environ. 144, 152–171. https://doi.org/10.1016/j.rse.2014.01.011.